

1 An analytical method to estimate groundwater
2 depletion of an aquitard due to variable drawdowns
3 in adjacent aquifers

4 **Zhaofeng Li**^{1,2,3*}, **Hao Li**¹, **Xianxuan Xiao**^{1,2}, **Walter A. Illman**³, and **Ruizhe**
5 **Wang**¹

6 ¹ College of Environment and Civil Engineering, Chengdu University of Technology,
7 Chengdu 610059, China

8 ² State Key Laboratory of Geohazard Prevention and Geoenvironment Protection
9 (Chengdu University of Technology), Chengdu 610059, China

10 ³ Department of Earth & Environmental Sciences, University of Waterloo, Waterloo,
11 Ontario, Canada

12 Corresponding author: Zhaofeng Li (lizhaofeng17@cdut.edu.cn)

13 **Key points:**

- 14 • Analytical solution of drawdown in an aquitard corresponding to variable
15 drawdowns is derived.
- 16 • An analytical method to estimate groundwater depletion from an aquitard is
17 proposed.
- 18 • Corresponding type-curve fitting method is developed to estimate hydraulic
19 parameters.
- 20 • Analysis of factors contributing to aquitard deformation is presented.

21 **Keywords:** Nonlinear consolidated aquitard; Groundwater depletion; Variable
22 drawdowns; Type-curve fitting method; Groundwater storage assessment

23 **Abstract**

24 Computing aquitard depletion, which is often overlooked, is of great
25 significance for the assessment of groundwater resources and land subsidence. The
26 issue is viewed as troublesome because of the additional computational burden, the
27 poorly known hydrogeological parameters of the aquitard, and the lack of drawdown
28 history in pumped aquifers. In this study, an analytical solution is derived to describe
29 the drawdown variation in a nonlinear-consolidated aquitard under the condition of
30 variable drawdowns in adjacent aquifers. Based on the analytical solution, we study
31 the characteristics of groundwater dynamics and water balance under the conditions of
32 linearly increasing drawdown of aquifers in adjacent aquifers. In addition, we put
33 forward a method to calculate the depletion and hydrogeological parameters of an
34 aquitard corresponding to variable drawdowns in adjacent aquifers, applicable even
35 when historical drawdown data are lacking. The accuracy of the method is generally
36 very good, but results improve when the drawdown history of pumped aquifers is
37 divided into more periods for estimation. Under the condition of linear drawdown in
38 adjacent aquifers, groundwater depletion and maximum water release rate of the
39 aquitard increases with increasing compression index, coefficient of consolidation,
40 aquitard thickness, rate of drawdown change in the adjacent aquifer, while decreasing
41 with initial void ratio, and initial effective stress. The proposed approach is
42 demonstrated at a field site in Shanghai City of China, and it would help for the

43 effective management of groundwater resources and estimation of the global transfer
44 from groundwater to surface water.

45 **1. Introduction**

46 Groundwater is generally overexploited over the world due to the increasing
47 demand for water resources, and it has brought a series of environmental problems,
48 including the decline of groundwater levels, land subsidence (Li et al., 2021; Shi et al.,
49 2007; Shi et al., 2008) and sea level rise (Konikow & Kendy, 2005). A multi-layered
50 aquifer system in the sedimentary plain area, such as the Dakota aquifer system in the
51 United States and the Yangtze Delta in China (Guo & Li, 2015; Ye et al., 2016),
52 usually consists of multiple aquifers with alternating aquitards in between (Zhuang et
53 al., 2015). Water stored in aquitards is a significant source of pumped aquifers, and it
54 tends to be more storable than confined aquifers (Liu et al., 2022; Zhang et al., 2020a).
55 Meanwhile, aquitard storage is difficult to recover and could often be the primary
56 source of groundwater released from the storage of aquifer systems (Shi et al., 2008).
57 Consequently, the accurate calculation of groundwater depletion in aquitards is
58 essential for the effective management of groundwater resources, and it would help
59 estimate the global transfer of groundwater to surface water (Konikow & Neuzil,
60 2007).

61 Due to low hydraulic conductivity and non-negligible specific storage, water
62 release from aquitards and its deformation always lag behind the drawdown in
63 adjacent confined aquifers (Bakr, 2015; Liu et al., 2022; Ye et al., 2016). Zhou et al.
64 (2013) studied the groundwater dynamics and water balance of an aquitard, while the

drawdown was a constant amount in an adjacent confined aquifer. The hydraulic head in aquifers lying above or under the aquitard usually decreased with increasing groundwater extraction (Custodio, 2002), Neuman & Gardner (1989) presented convolution integrals for calculating the drawdown in the aquitard under the condition of water table fluctuation. A widely applicable method was proposed to estimate the groundwater depletion of the aquitard in the entire or limited period of exploitation history, especially when the data on drawdown of history is sufficient (Li & Zhou, 2015; Li et al., 2017). Konikow & Neuzil (2007) presented a simplified method to estimate the groundwater depletion from the confining layers in response to withdrawals from adjacent aquifers. Alternatively, given the same information, a well-calibrated, numerical simulation model (i.e., three-dimensional model such as MODFLOW can be used to compute the groundwater depletion of aquitards in response to pumping of aquifers (Arabameri et al., 2020; Burbey, 2020; Zhang et al., 2020b).

Most of the aforementioned studies were carried out based on the one-dimensional consolidation theory for saturated clays (Terzaghi, 1943), which assumed the aquitard hydraulic parameters being constant values. However, in reality, hydraulic parameters decrease nonlinearly during the consolidation process of the aquitard, which is contrary to the assumption of Terzaghi's theory, and Terzaghi's model often leads to unexpected differences between theoretical results and field observations (Davis & Raymond, 1965; Gibson et al., 1967; Xie & Leo, 2004). Li et al. (2018) and Luo et al. (2020) proposed analytical solutions to characterize the water

release from a one-dimensional large-strain aquitard and a nonlinearly consolidated aquitard, respectively, subjected to an abrupt hydraulic head decline in adjacent confined aquifers.

The accuracy of water depletion calculation of the aquitard storage relies to a large degree on the accuracy of aquitard hydraulic parameters, which can be determined by the results of laboratory and in-situ experiments (Burbey, 2020; Zhang et al., 2020b; Zhao et al., 2019). Zhou et al. (2013) used an analytical method to calculate aquitard hydraulic parameters while the drawdown in the adjacent aquifer was constant. Burbey (2003) characterized the specific storage and hydraulic conductivity of the aquitard by taking advantage of time-subsidence data during a pumping test with a graphical technique. (Zhang et al., 2015); Zhuang et al. (2015) proposed a type-curve method for estimating the hydraulic conductivity and the specific storage of an aquitard in a multi-layered aquifer system by using data on aquitard compaction and drawdown history of aquifers. Luo et al. (2020) calculated the hydraulic parameters of the aquitard undergoing non-linear consolidation using a laboratory experiment while the drawdown in the adjacent aquifer was constant. In addition, Konikow & Neuzil (2007) demonstrated a general relationship between porosity and hydraulic conductivity considering the clay content of the aquitard and the relation between porosity and specific storage considering the consolidation degree.

In short, it is difficult to calculate the water depletion of the aquitard because of the complex drainage process and poorly known hydraulic parameters of the aquitard,

109 and the paucity of drawdown data within the pumped aquifer, especially during the
110 early stage of groundwater exploitation and in developing countries. In this study, we
111 present an analytical solution to describe the drawdown in an aquitard for an arbitrary
112 drawdown of adjacent confined aquifers. Based on the analytical solution, we also
113 develop methods to calculate the hydrogeological parameters and the long-term
114 decreases in the volume of water stored in an aquitard undergoing nonlinear
115 consolidation, under a condition that the drawdown history of the aquifers lying above
116 and below the aquitard can be approximated as a step-by-step piecewise function with
117 respect to time, in each of which the drawdown is a constant amount. The new method
118 proposed in this study is demonstrated through a laboratory experiment and a field
119 application to the aquifer system beneath Shanghai city of China. The hydraulic
120 parameters determined by the method in this study are compared with the geological
121 method of Konikow & Neuzil (2007). The results of the laboratory experiment and
122 field applications demonstrate the correctness and accuracy of the approach in this
123 study.

124 **2. Mathematical Model and Analytical Method**

125 **2.1 The Governing Equation of Drawdown in the Aquitard**

126 Hydraulic head in an aquifer alters the boundary conditions for the adjoining
127 aquitard, causing it to release water from storage to the aquifer as drawdown
128 propagates slowly into the aquitard. Despite the low permeability nature of aquitards,
129 relatively large specific storage values in clay-rich aquitards can enable large
130 quantities of water to “leak” into aquifers over long timescales (Konikow & Neuzil,

2007). To study the water amount released from the aquitard, a multi-layered aquifer system was considered. The Lagrangian coordinate a was used, which was assumed to be positive in a vertically downward direction, with the coordinate origin located at the top surface of the aquitard (Figure 1).

The system is composed of an aquitard and aquifers on both sides, of which horizontal length is infinite. The hydraulic conductivity of each aquifer exceeds that of the aquitard by at least two orders of magnitude. As seepage in the aquitard follows the path of least resistance, water flow in the confining layer is essentially vertical (Neuman & Gardner, 1989; Neuman & Witherspoon, 1969; Zhang et al., 2015).

Figure 1. Conceptual model of the multi-layered aquifer-aquitard system.

The assumptions of one-dimensional nonlinear consolidation theory are as follows: (1) The horizontal length of the aquitard is infinite and its initial thickness is l ; (2) the aquitard is homogeneous and saturated; (3) individual clay particles and the pore water in the aquitard are incompressible during consolidation; (4) the groundwater flow in the aquitard is one-dimensional, vertical and follows Darcy's law; (5) soil creeping is not considered, and the nonlinear variations of aquitard compressibility during the consolidation process are assumed to abide by equation (1).

$$e = e_0 - C_c \log_{10}(\sigma' / \sigma'_0) \quad \#(1)$$

where the soil compression index C_c is assumed to be constant (dimensionless), and is approximately valid; e is the void ratio in the aquitard at position a and time t (dimensionless); e_0 is the initial void ratio of the aquitard (dimensionless); σ' is the

153 vertical effective stress ($\text{ML}^{-1}\text{T}^{-2}$); and σ'_0 is the initial effective stress ($\text{ML}^{-1}\text{T}^{-2}$). (6)

154 The coefficient of aquitard compressibility (m_v) can be given by:

155
$$m_v = -\frac{1}{1+e} \frac{de}{d\sigma'} = \frac{0.434C_c}{(1+e)\sigma'} \#(2)$$

156 where the change of $(1+e)$ with time during the consolidation process is much
157 smaller than the σ' , so for any load increment, $(1+e)$ can be regarded as a constant
158 (Luo et al., 2020). Because the variation of e is much smaller than the variation of σ' ,
159 the coefficient of consolidation c_v is considered to be relatively constant (Davis &
160 Raymond, 1965). This is equivalent to assuming that the decrease in m_v is
161 proportional to the decrease in hydraulic conductivity k_v during the consolidation
162 process of the aquitard.

163
$$c_v = \frac{k_v}{m_v \gamma_w} \#(3)$$

164 where, γ_w is unit weight of water.

165 A nonlinear large deformation consolidation equation (Gibson's theory) with a
166 void ratio as control variable is given by Gibson et al. (1967); (Gibson et al., 1981),
167 while the self-weight of the soil is ignored (Luo et al., 2020).

168
$$\frac{\partial}{\partial a} \left[\frac{k_v(1+e_0)}{\gamma_w(1+e)} \frac{d\sigma'}{de} \frac{\partial e}{\partial a} \right] + \frac{1}{(1+e_0)} \frac{\partial e}{\partial t} = 0 \#(4)$$

169 Substituting equations (1), (2) and (3) into equation (4) to obtain the governing
170 equation of depletion of the aquitard undergoing nonlinear consolidation:

171
$$c_v \left[\frac{\partial^2 \sigma'}{\partial a^2} - \frac{1}{\sigma'} \left(\frac{\partial \sigma'}{\partial a} \right)^2 \right] = \frac{\partial \sigma'}{\partial t} \#(5)$$

172 In addition, according to the principle of effective stress(Terzaghi, 1943),

173
$$\sigma' = \sigma'_0 + \gamma_w s \#(6)$$

174 where s is the drawdown in adjacent aquifers.

175 For the thin soil layer, the weight of the soil layer can be ignored, and the initial
 176 effective stress (σ'_0 , geostatic stress) is distributed uniformly through the entire
 177 thickness, and the accuracy of calculation is poor while the thickness of aquitard is
 178 large (Gibson et al., 1967; Gibson et al., 1981). Substituting equation (6) into equation
 179 (5) leads to a governing equation describing nonlinear consolidation of an aquitard.

$$c_v \left[\frac{\partial^2 s}{\partial a^2} - \frac{\gamma_w}{\sigma'_0 + \gamma_w s} \left(\frac{\partial s}{\partial a} \right)^2 \right] = \frac{\partial s}{\partial t} \quad \#(7)$$

180 It is assumed that the initial drawdown distribution in the aquitard is a function
 181 $f(a)$ of position a , which is caused by a previous external force disturbance, and the
 182 drawdown in the aquifers lying above and under the aquitard are $s_0(t)$ and $s_1(t)$,
 183 which are functions of time t , at $a = 0$ and $a = l$, respectively. To obtain the
 184 drawdown in the aquitard, the following initial and boundary conditions are needed.

$$s(a, 0) = f(a) \quad 0 < a < l \quad \#(8)$$

$$s(0, t) = s_0(t) \quad t > 0 \quad \#(9)$$

$$s(l, t) = s_1(t) \quad t > 0 \quad \#(10)$$

188 2.2 Analytical Solutions

189 The solution to equations (7)-(10) can be derived by variable transformation and
 190 the characteristic function method. Details to the derivation of the mathematical
 191 model are listed in the Appendix. The drawdown variation in the aquitard is given as,

$$s(a, t) = \frac{\sigma'_0}{\gamma_w} (10^{w(a,t)} - 1) \quad \#(11)$$

192 Where:

$$\begin{aligned}
w(a, t) &= \sum_{n=1}^{\infty} \left[T_n(0) e^{-\frac{n^2 \pi^2 c_v t}{l^2}} + e^{-\frac{n^2 \pi^2 c_v t}{l^2}} \int_0^t f_n(t) e^{\frac{n^2 \pi^2 c_v t}{l^2}} dt \right] \sin \frac{n\pi a}{l} \\
&\quad + \log_{10} \frac{\sigma'_0 + \gamma_w s_0(t)}{\sigma'_0} + \frac{a}{l} \log_{10} \frac{\sigma'_0 + \gamma_w s_1(t)}{\sigma'_0 + \gamma_w s_0(t)} \\
T_n(0) &= \frac{2}{l} \int_0^l \log_{10} \frac{\sigma'_0 + \gamma_w f(a)}{\sigma'_0} \sin \frac{n\pi a}{l} da \sin \frac{n\pi a}{l} \\
&\quad + \frac{2}{n\pi} \left(\log_{10} \frac{\sigma'_0 + \gamma_w s_1}{\sigma'_0} (-1)^n - \log_{10} \frac{\sigma'_0 + \gamma_w s_0}{\sigma'_0} \right) \\
f_n(t) &= \frac{2}{n\pi \ln 10} \left[\frac{(-1)^n \gamma_w}{\sigma'_0 + \gamma_w s_1(t)} \frac{\partial s_1(t)}{\partial t} - \frac{\gamma_w}{\sigma'_0 + \gamma_w s_0(t)} \frac{\partial s_0(t)}{\partial t} \right]
\end{aligned}$$

193 and s_0 and s_1 are the abrupt drawdown in the aquifers above and under the aquitard at
194 the initial time, respectively.

195 According to Darcy's law, the flux per unit horizontal area at position a and at
196 time t is given by $q(a, t) = k(\partial s / \partial a)$. According to the principle of water balance,
197 the leakage rate of aquitard per unit horizontal area $q(t)$, which is equal to the $q(a, t)$
198 at location $a = l$ minus that at location $a = 0$ at time t can be expressed by equation
199 (12).

$$q(t) = \frac{c_c c_v}{(1 + e_0)l} \frac{\partial w}{\partial a} \quad \#(12)$$

200 The hydraulic head of the pumped aquifer often varies both temporally and
201 spatially (Neuman & Gardner, 1989). Sometimes, the drawdown may increase
202 linearly with time (Zhuang et al., 2015). However, most regions lack data on
203 drawdown history of pumped aquifers, especially in developing countries (Konikow
204 & Neuzil, 2007) and during the early stage of groundwater exploitation (Shi et al.,
205 2008) due to scarcity in monitoring technology to sustainably extract groundwater. In
206 addition, the solution (equations (11) and (12)) includes terms of integration and

207 derivation, which makes the calculation difficult.

208 Here, the temporal variations of drawdown history with sparse data were
 209 considered and the drawdown history was separated into many periods, each of which
 210 the drawdown is constant and is defined as $\varphi_{0,i}$ and $\varphi_{1,i}$ ($i=1, 2 \dots m$) for the aquifers
 211 lying above and under the aquitard, respectively (Figure. 2). Namely, $s_0(t)$ and $s_1(t)$
 212 were defined as a piecewise continuous step function (equation (13)). Meanwhile, to
 213 improve the accuracy of the estimation method, we quote the value of “Representative
 214 time” in each period of the drawdown history, “If the rate of drawdown is relatively
 215 stable over time, when the time of fixed drawdown is half that of linear drawdown,
 216 the water release from consolidation is basically the same” (Konikow & Neuzil,
 217 2007). The history of the hydraulic head decline of adjacent aquifers and the step
 218 changes in hydraulic head for the analytical solutions are shown in Figure 2.

$$[s_0(t), s_1(t)] = \begin{cases} [\varphi_{0,1}, \varphi_{1,1}] & t_0 \leq t \leq t_1 \\ [\varphi_{0,2}, \varphi_{1,2}] & t_1 \leq t \leq t_2 \\ \dots \dots & \dots \dots \\ [\varphi_{0,m}, \varphi_{1,m}] & t_{m-1} \leq t \leq t_m \end{cases}, m \geq 1 \#(13)$$

219

220 **Figure 2. Drawdown versus time defined as a step-by-step piecewise function.**

221 The leakage rate of the aquitard per unit horizontal area (L^3T^{-1}) caused by
 222 variable drawdown in adjacent aquifers, which are step-by-step piecewise functions
 223 with respect to time, is obtained by substituting equation (13) into equation (12),
 224 given as,

$$q(\bar{t}) = \frac{C_c C_v}{(1 + e_0) l} \bar{q}(\bar{t}) \#(14)$$

225 where $\bar{t} = \frac{c_v t}{l^2}$,

$$\bar{q}(\bar{t}) = 2 \sum_{i=0}^{m-1} \sum_{n=1}^{\infty} [(-1)^n - 1] \left((-1)^n \log_{10} \frac{\sigma'_{1,i+1}}{\sigma'_{1,i}} - \log_{10} \frac{\sigma'_{0,i+1}}{\sigma'_{0,i}} \right) e^{-n^2 \pi^2 (\bar{t}_m - \bar{t}_i)} \quad ,$$

$$\sigma'_{0,i} = \sigma'_0 + \gamma_w \varphi_{0i} \text{ and } \sigma'_{1,i} = \sigma'_0 + \gamma_w \varphi_{1i}.$$

The cumulative water released from the aquitard per unit horizontal area $Q(\bar{t})$ (L^3) can be obtained through the integration of $q(\bar{t})$ over time.

$$Q(\bar{t}) = \int q(\bar{t}) d\bar{t} = \frac{C_c l}{(1 + e_0)} \bar{Q}(\bar{t}) \quad (15)$$

$$\text{where } \bar{Q}(\bar{t}) = 2 \sum_{i=0}^{m-1} \sum_{n=1}^{\infty} \frac{[1 - (-1)^n]}{n^2 \pi^2} \left((-1)^n \log_{10} \frac{\sigma'_{1,i+1}}{\sigma'_{1,i}} - \log_{10} \frac{\sigma'_{0,i+1}}{\sigma'_{0,i}} \right) (1 - e^{-n^2 \pi^2 (\bar{t}_m - \bar{t}_i)}).$$

The above analytical method can be used to estimate the water release from the aquitard due to fluctuating hydraulic head in adjacent aquifers, especially lacking the drawdown history data during the early stage of groundwater exploitation. Compared with the solutions based on Terzaghi's theory (Li et al., 2017), the solution (equation 11) in this study considers the nonlinear change of compressibility and permeability during aquitard consolidation. Therefore, the proposed method is more practical and accurate for the purposes of estimating groundwater resources and the corresponding consolidation problem compared to traditional linear theory. In addition, we are interested in a relatively compressible aquitard and can ignore the compressibility of water and soil particles. Consequently, land subsidence caused by the depletion of groundwater stored in aquitard equals the value of Q . This method can be used to determine the hydrogeological parameters with data of aquitard deformation and drawdown in adjacent aquifers.

3. Testing and Verification of the Analytical Solution

3.1 Analytical Solution under Abrupt Drawdown in Adjacent Aquifers

In this case, it is assumed that the hydraulic head distribution in the aquitard is

247 uniform at initial time, and the hydraulic head in the aquifer underlying the aquitard is
 248 constant, namely, $s(l, t) = \varphi$, and the drawdown in the aquifer overlying the aquitard
 249 is constant ($s(0, t) = 0$ or φ). Substituting these boundary and initial conditions into
 250 equation (15), the Q (L^3) of the aquitard undergoing drainage from one or both sides
 251 with constant drawdown are obtained respectively, as equation (16a) and (16b).

$$Q(\bar{t}) = \frac{2C_c l}{(1 + e_0)} \log_{10} \left(\frac{\sigma'_f}{\sigma'_0} \right) \sum_{n=1}^{\infty} \frac{[1 - (-1)^n]}{n^2 \pi^2} (1 - e^{-n^2 \pi^2 \bar{t}}) \# (16a)$$

$$Q(\bar{t}) = \frac{4C_c l}{(1 + e_0)} \log_{10} \left(\frac{\sigma'_f}{\sigma'_0} \right) \sum_{n=1}^{\infty} \frac{[1 - (-1)^n]}{n^2 \pi^2} (1 - e^{-n^2 \pi^2 \bar{t}}) \# (16b)$$

252 By comparing the Q of the aquitard undergoing drainage from one side
 253 (equation (16a)) with those of the aquitard undergoing drainage from both sides
 254 (equation (16b)), it can be found that the Q from the aquitard undergoing drainage
 255 from both sides is twice that of the aquitard undergoing drainage from one side, while
 256 the drawdown of aquifers on both sides of the aquitard is the same.

257 To determine the hydrogeological parameters of the aquitard, while the
 258 drawdown increases by φ in the adjacent aquifer, the logarithmic forms of equations
 259 (16a) and (16b) in a dimensionless form (\bar{Q}) and dimensionless time (\bar{t}) are
 260 respectively expressed as:

$$\log_{10} \bar{Q}(\bar{t}) = \log_{10} Q(t) + \log_{10} \left[\frac{(1 + e_0)}{C_c l \log(\sigma'_f / \sigma'_0)} \right] \# (17a)$$

$$\log_{10} \bar{t} = \log_{10} t + \log_{10} \frac{c_v}{l^2} \# (17b)$$

261 The type-curve approach is used to calculate the hydraulic parameters of the
 262 aquitard. Since the second term of the equation is a constant in the logarithmic plot,
 263 the data curve of the flux $Q(t)$ is analogous to the type-curve of the dimensionless

264 deformation \bar{Q} . The method involves the following steps: 1) superimpose the $Q(t)$
 265 curve on $\bar{Q}(\bar{t})$, while the axes of the two figures remain parallel; 2) Select any
 266 intersection of standard curve and $Q(t)$ test curve as the match point; and 3) then, the
 267 coordinates of the match points ($Q(t)$, $\bar{Q}(\bar{t})$, t and \bar{t}) are substituted into equations (18)
 268 and (19) to determine the parameters.

$$c_v = \frac{\bar{t}}{t} \cdot l^2 \#(18)$$

$$C_c = \frac{Q(t)(1 + e_0)}{\log_{10} \left(\frac{\sigma'_f}{\sigma'_0} \right) \bar{Q}(\bar{t})l} \#(19)$$

269 3.2 Experimental test and Verification

270 To test the applicability of the formula and to verify the type-curve fitting
 271 method, the consolidated drainage data from Luo et al. (2020) are used in the study. A
 272 consolidation test of aquitard undergoing drainage from one side was carried out
 273 when the drawdown in the adjacent aquifer increases abruptly. The consolidation
 274 container is a cylinder with an inner diameter of 0.384 m, which is made of organic
 275 glass. The soil layer is divided into three layers from top to bottom: A middle silty
 276 clay layer with thickness of 0.24 m represented the aquitard. ($l = 0.24$ m), and its
 277 basic parameters are: $e_0 = 0.869$ and $\sigma'_0 = 2.77$ kPa. The thicknesses of the upper and
 278 lower sand aquifers were 0.220 and 0.165 m. During the laboratory test, a constant
 279 decrease in hydraulic head of $\varphi = 1$ m was maintained, and the water depletion (Q)
 280 of the clay layer was recorded during the experiment.

281 The $Q(t)$ data curve and the type-curve of $\bar{Q}(\bar{t})$ are plotted in Figure 3, and
 282 superimposed by keeping the axes of the two graphs parallel to each other (Figure 3).

283 The coordinates of the match point are $Q = 4.6 \times 10^{-4} \text{ m}^3$, $\bar{Q} = 0.280$, $t = 2.8 \times 10^3 \text{ s}$, and
 284 $\bar{t} = 0.076$. The computed c_v and C_c are $1.56 \times 10^{-6} \text{ m}^2/\text{s}$, 0.1496, respectively, by
 285 substituting these coordinates into equations (18) and (19). The specific storage S_s and
 286 k_v of the clay layer at the initial time are 0.125, $1.953 \times 10^{-7} \text{ m/s}$ calculated by
 287 $S_s = \frac{0.434\gamma_w C_c}{(1+e_0)\sigma'_0}$ and $k_v = \frac{0.434c_v C_c \gamma_w}{(1+e_0)\sigma'_0}$, respectively. The hydraulic parameters
 288 determined in this study are basically equal to that calculated by Luo et al. (2020).

289 Figure 4 compares the measured depletion within the observation time of the
 290 clay layer and the results predicted by substituting these estimated parameters into the
 291 equation (16a) proposed in this study and the studies of Li et al. (2018) and Zhou et al.
 292 (2013). $Q(t)$ predicted by the analytical solution ($7.15 \times 10^{-4} \text{ m}^3$) in this study agrees
 293 well with the experimental results ($7.11 \times 10^{-4} \text{ m}^3$), and the $Q(t)$ predicted by the
 294 solutions in the studies of Li et al. (2018) and Zhou et al. (2013) are 1.03×10^{-3} and
 295 $1.71 \times 10^{-3} \text{ m}^3$, respectively, which is larger than the measured deformation of the clay
 296 layer.

297

298 **Figure 3. Determination of parameters by the type-curve fitting method.**

299

300 **Figure 4. Comparison of predicted and measured fluxes and settlement of the soil.**

301 **4. Evaluation and Discussion**

302 **4.1 Analytical Solutions under the Linear Drawdown in the Adjacent Aquifers**

303 It is assumed that the hydraulic head distribution in the aquitard is uniform at
 304 initial time ($s(a, 0) = 0$), and the drawdown in the aquifers above and below the

305 aquitard both increases linearly. Namely, the boundary conditions of the equation (7)
 306 are $s(0, t) = \beta_1 t$ and $s(l, t) = \beta_2 t$ (where β_1 and β_2 are the rate of drawdown in
 307 the aquifer overlying and underlying the aquitard, respectively) at the positions of $a =$
 308 0 and $a = l$, respectively. Substituting these boundary conditions and initial condition
 309 into equation (12), the $q(t)$ of the aquitard undergoing drainage from both sides under
 310 the condition of linear drawdown is obtained,

$$311 \quad q(t) = \frac{c_v C_c}{(1+e_0)l} \left\{ \frac{2}{\ln 10} \sum_{n=1}^{\infty} [(-1)^n - 1] \left[e^{-\frac{n^2 \pi^2 c_v t}{l^2}} \int_0^t \left(\frac{(-1)^n \gamma_w \beta_2}{\sigma'_0 + \gamma_w \beta_2 t} - \frac{\gamma_w \beta_1}{\sigma'_0 + \gamma_w \beta_1 t} \right) e^{\frac{n^2 \pi^2 c_v t}{l^2}} dt \right] \right\} \#(20)$$

312 The $Q(t)$ of the aquitard undergoing drainage from both sides under the
 313 condition of linear drawdown is derived through integration of $q(t)$ over time.

$$314 \quad Q(t) = \frac{c_v C_c}{(1+e_0)l} \frac{2}{\ln 10} \sum_{n=1}^{\infty} [(-1)^n - 1] \int_0^t \left[e^{-\frac{n^2 \pi^2 c_v t}{l^2}} \int_0^t \left(\frac{(-1)^n \gamma_w \beta_2}{\sigma'_0 + \gamma_w \beta_2 t} - \frac{\gamma_w \beta_1}{\sigma'_0 + \gamma_w \beta_1 t} \right) e^{\frac{n^2 \pi^2 c_v t}{l^2}} dt \right] dt \#(21)$$

315 4.2 Accuracy Evaluation

316 The proposed analytical method was tested and evaluated by application to a
 317 hypothetical system with specified hydraulic properties and boundary conditions. The
 318 $Q(t)$ of the aquitard undergoing drainage from both sides are twice that of the
 319 aquitard undergoing drainage from one side, while the drawdown of aquifers on both
 320 sides of the aquitard is the same. Here, we only analyze the water release of the
 321 aquitard undergoing drainage from one side shown as in Figure 1. Substantial
 322 groundwater withdrawal from wells in the underlying confined aquifer caused a linear
 323 increase in drawdown, which in turn induced depletion from the aquitard. According
 324 to the previous study (Li et al., 2019), the parameters used in this section are: $C_c =$
 325 0.054, $\sigma'_0 = 51$ kPa, $e_0 = 1.10$, $c_v = 1.10 \times 10^{-7}$ m/s², $\beta = 1$ m/year, and $l = 10$ m.

326 A comparison was made between the solutions of $Q(t)$ of the aquitard under the
 327 linear drawdown condition (equation (21)) and that estimated by the proposed
 328 analytical method (equation (15)) under the stepped drawdown condition. In order to
 329 evaluate the accuracy of the proposed method, we divided the drawdown history of
 330 the pumped aquifer into different numbers of periods to calculate the aquitard
 331 depletion. As shown in Figure 6, the $Q(t)$ predicted by equation (21) increases over
 332 time and it is 0.0473 m^3 at 10 years. The $Q(t)$ at 10 years predicted by equation (15)
 333 were 0.0492 , 0.0480 and 0.0478 m^3 , while the drawdown history of the pumped
 334 aquifer is divided into 1, 2 and 3 periods, respectively. The $Q(t)$ at 10 years as
 335 predicted by equation (15) is slightly greater than that predicted by equation (21), and
 336 the errors are about 4.02% , 1.47% and 1.05% for 1, 2 and 3 periods, respectively.
 337 Therefore, the accuracy of the proposed analytical method is very good for estimating
 338 groundwater depletion from the aquitard, and it is better while the period number of
 339 drawdown history increases.

340

341 **Figure 5. The Cumulative amount of water released from the aquitard.**

342 4.3 Parametric sensitivity for water release rate and depletion of aquitard

343 In order to investigate the effect of hydraulic parameters on the depletion from
 344 an aquitard under the condition of increasing drawdown, we conduct a parametric
 345 sensitivity analysis of the aquitard depletion, by varying the values in sections 4.2 at a
 346 time. This section analyzed the effect of the C_c , e_0 , c_v , $\sigma'_0 l$ and β on water release rate
 347 and depletion of the aquitard undergoing drainage from one side. In addition, we

348 compared the water release under the conditions of linear drawdown and fixed
349 drawdown in the adjacent aquifer, and we take half of the total time as the
350 “Representative time” while calculating the water depletion of the aquitard when the
351 drawdown in the adjacent aquifer increases abruptly (Konikow & Neuzil, 2007).

352

353 **Figure 6. The water release rate of the aquitard with the linear drawdown in the pumped**
354 **aquifer for different values of (a) C_c (b) e_0 , (c) c_v , (d) σ'_0 , (e) l and (f) β .**

355 The $q(t)$ of the aquitard under the conditions of linear drawdown is predicted
356 by equation (20) (see Figure 6). The $q(t)$ increases rapidly to a maximum initially,
357 then it decreases, and the rate of decrease gradually slows down. The variation of $q(t)$
358 under different values of parameters also increases to a maximum initially, then it
359 gradually decreases. Namely, the effect of the parameter values on $q(t)$ decreases
360 under the condition of the linear drawdown over long timescales.

361 The $q(t)$ of the aquitard draining from one side are calculated with different C_c
362 values (see Figure 6a). The $q(t)$ increases with increasing C_c , and the occurrence time
363 for the maximum value of $q(t)$ does not depend on the value of C_c . The maximum
364 values of $q(t)$ are 5.11×10^{-3} , 1.02×10^{-2} , 1.53×10^{-2} , 2.04×10^{-2} m³/year, while the
365 corresponding values of C_c are 0.05, 0.10, 0.15 and 0.20, respectively, and the
366 occurrence time for the $q(t)$ maximum value is 4.2 years.

367 The $q(t)$ of the aquitard draining from one side are calculated with different e_0
368 values (see Figure 6b). The $q(t)$ decreases with increasing e_0 , and the occurrence time
369 for the maximum value of $q(t)$ does not depend on the value of e_0 . The maximum

values of $q(t)$ are 7.72×10^{-3} , 5.79×10^{-2} , 4.63×10^{-2} , 3.89×10^{-2} m³/year, while the corresponding values of e_0 are 0.5, 1.0, 1.5 and 2.0, respectively, and the occurrence time for the $q(t)$ maximum value is 3.85 years.

The $q(t)$ of the aquitard draining from one side are calculated with different c_v values (see Figure 6c). The $q(t)$ is greater with a larger value of c_v at the initial stage, and then it is less with a larger value of c_v . The occurrence time for the maximum value of $q(t)$ decreases with an increasing c_v . The maximum values of $q(t)$ are 5.36×10^{-3} , 6.57×10^{-3} , 8.00×10^{-3} , 8.83×10^{-3} m³/year, and the occurrence time for the $q(t)$ maximum values are 4.35, 2.85, 1.4 and 0.95 years, while the corresponding values of c_v are 1×10^{-7} , 2×10^{-7} , 5×10^{-7} and 1×10^{-6} m²/s, respectively. The $q(t)$ are 1.03×10^{-3} , 9.99×10^{-4} , 9.83×10^{-4} , 9.78×10^{-4} m³/year at the 50th year, while the corresponding values of c_v are 1×10^{-7} , 2×10^{-7} , 5×10^{-7} and 1×10^{-6} m²/s, respectively.

The $q(t)$ of the aquitard draining from one side are calculated with different σ'_0 values (see Figure 6d). The $q(t)$ decreases with an increasing σ'_0 , and the occurrence time for the maximum value of $q(t)$ increases with an increasing σ'_0 . When the σ'_0 values are 50, 100, 150 and 200 kPa, the maximum values of $q(t)$ are 1.46×10^{-2} , 9.99×10^{-3} , 5.53×10^{-3} and 3.42×10^{-3} m³/year, and the occurrence time for $q(t)$ maximum values are 2.10, 2.75, 4.15, 5.25 years, respectively.

The $q(t)$ of the aquitard draining from one side are calculated with different l values (see Figure 6e). The $q(t)$ increases with an increasing l , and the occurrence time for the maximum value of $q(t)$ increases with an increasing l . When the values of l are 5, 10, 15 and 20 m, the maximum values of $q(t)$ are 3.91×10^{-3} , 5.50×10^{-3} ,

392 6.18×10^{-3} , 6.44×10^{-3} m³/year, and the occurrence time for $q(t)$ maximum values are
393 1.75, 3.65, 6.45, 9.50 years, respectively.

394 The $q(t)$ of the aquitard draining from one side are calculated with different β
395 values (see Figure 6f). The $q(t)$ increases with an increasing β , and the occurrence
396 time for the maximum value of $q(t)$ decreases with an increasing β . While the values
397 of β are 0.5, 1, 1.5 and 2 m/year, the maximum values of $q(t)$ are 3.06×10^{-3} , 5.36×10^{-3} ,
398 6.57×10^{-3} and 7.86×10^{-3} m³/year, and the occurrence time for $q(t)$ maximum values
399 are 5.32, 4.45, 3.55 and 3.15 years, respectively.

400

401 **Figure 7. Depletion of the aquitard with a linear drawdown in the pumped aquifer for**
402 **different values of (a) L , (b) c_v , (c) σ'_0 , and (d) β_1 .**

403 The depletion of the aquitard under the conditions of linear drawdown and
404 constant drawdown, which are respectively predicted through equations (21) and
405 (16a), increases with an increasing C_c (Figure 7a), and the difference of $Q(t)$ between
406 the two cases increases with an increasing C_c . In particular, the estimated depletion of
407 the aquitard under the linear drawdown conditions are 0.116, 0.231, 0.347, 0.463 m³,
408 and that under the constant drawdown conditions are 0.118, 0.236, 0.354, 0.472 m³,
409 which are 0.05, 0.10, 0.15 and 0.20, for corresponding values of C_c , respectively, and
410 the error of the estimation method is 2.03%.

411 The $Q(t)$ of the aquitard draining from one side are calculated with different e_0
412 values (see Figure 7b). The $Q(t)$ predicted under the conditions of linear drawdown
413 and constant drawdown decreases with an increasing e_0 and the difference of aquitard

414 depletion between two cases decreases with an increasing value of e_0 . In particular,
 415 the estimated depletion of the aquitard under the linear drawdown conditions are
 416 0.175, 0.131, 0.105, 0.0874 m³, and that under the constant drawdown condition are
 417 0.179, 0.134, 0.107, 0.0875 m³, which are 0.5, 1.0, 1.5 and 2.0, for corresponding
 418 values of e_0 , respectively, and the error of the estimation method is 2.28%.

419 The $Q(t)$ of the aquitard draining from one side are calculated with different c_v
 420 values (see Figure 7c). The $Q(t)$ increases slightly with an increasing c_v under the
 421 conditions of linear drawdown and constant drawdown decreases and the final $Q(t)$
 422 does not depend on c_v under the constant drawdown condition, while the
 423 consolidation rate accelerates with increasing c_v . In particular, the predicted depletion
 424 of the aquitard under the linear drawdown condition are 0.124, 0.126, 0.127 and 0.127
 425 m³, and that under the constant drawdown condition are 0.128 m³, and the errors are
 426 3.2%, 1.6%, 0.78%, 0.78% corresponding values of c_v , which are 1×10^{-7} , 2×10^{-7} ,
 427 5×10^{-7} and 1×10^{-6} m²/s, respectively.

428 The $Q(t)$ of the aquitard draining from one side are calculated with different σ'_0
 429 values (see Figure 7d). The $Q(t)$ predicted under the conditions of linear drawdown
 430 and constant drawdown decreases with an increasing σ'_0 and the difference of aquitard
 431 depletion between the two cases increases with an increasing σ'_0 . In particular, when
 432 the σ'_0 values are 50, 100, 150 and 200 kPa, the estimated depletion of the aquitard
 433 under the linear drawdown condition are 0.125, 0.0933, 0.0764, 0.0649 m³, and that
 434 under the constant drawdown condition are 0.128, 0.0960, 0.0787, 0.0672 m³, and the
 435 errors are 2.4%, 2.9%, 3.0% and 3.5%, respectively.

436 The $Q(t)$ of the aquitard draining from one side are calculated with different l
437 values (see Figure 7e). The $Q(t)$ predicted under the conditions of linear drawdown
438 and constant drawdown increases with an increasing l , and the difference of the $Q(t)$
439 between the two cases increases with an increasing value of l . In particular, when the
440 values of l are 5, 10, 15 and 20 m, the predicted $Q(t)$ under the linear drawdown
441 condition are 0.0636, 0.125, 0.182 and 0.229 m³, and that under the constant
442 drawdown condition are 0.0639, 0.128, 0.188 and 0.237 m³, and the errors are 3.1%,
443 3.2%, 3.3%, and 3.5% for corresponding values of l , respectively.

444 The $Q(t)$ of the aquitard draining from one side are calculated with different β
445 values (see Figure 7f). The $Q(t)$ predicted under the conditions of linear drawdown
446 and constant drawdown decreases with an increasing β , and the difference of aquitard
447 depletion between the two cases slightly decreases with an increasing β . When the
448 values of β are 0.5, 1, 1.5 and 2 m/year, the estimated depletion of the aquitard under
449 the linear drawdown condition are 0.0928, 0.125, 0.145 and 0.159 m³, and that under
450 the constant drawdown condition are 0.0953, 0.128, 0.148 and 0.162 m³, and the
451 errors are 2.8%, 2.1%, 1.4% and 1.2%, respectively.

452 **5. Field application**

453 **5.1 Hydrogeologic Setting**

454 The proposed method is also tested using data from a field site in Shanghai city,
455 China. Shanghai is a large metropolis located in the east of China and occupies an
456 area of nearly 6,340 km², (Figure 8). Shanghai City is underlain by a multi-layered
457 aquifer system composed of Quaternary sediments, with an average of 280 m (Zhang

et al., 2013). In 1860, Shanghai began to extract groundwater from deep wells, and land subsidence was first reported in 1921. The long-term over-exploitation of groundwater in aquifers has led to serious land subsidence (Shi et al., 2008; Zhang et al., 2007). The average total accumulated settlement in the city center was about 1.93 m, and the maximum was 2.63 m from 1921 to 2001 (Zhang et al., 2015).

To detect groundwater level changes and the compaction of individual strata, there are 27 extensometer groups and more than 1,400 observation wells in Shanghai (Figure 8) (Chai et al., 2004). The drawdown of hydraulic head in Shanghai can be divided into three stages. During the first stage, since the first observation of land subsidence in 1921, the continuous decline of groundwater level until 1965 led to a fast rate of land subsidence in Shanghai during this period, the net groundwater pumping rates and the average yearly rates of subsidence are $1.40 \times 10^8 \text{ m}^3/\text{year}$ and 32 mm/year. During the second stage, the pumping capacity decreased significantly from 1965 to 1981 to reduce the rate of land subsidence, and the average pumping capacity reached $0.38 \times 10^8 \text{ m}^3/\text{year}$. Moreover, due to large-scale artificial recharge of groundwater being carried out in the central urban area, the annual land subsidence rate resulted in a negative growth to -3mm/year. During the third stage, due to rapid economic development, the amount of groundwater exploitation increased and the groundwater level decreased slowly after 1981, but it was still higher than the groundwater level in the 1960s. The net groundwater pumping rates and the average yearly rates of subsidence are $1.13 \times 10^8 \text{ m}^3/\text{year}$ and 8.2 mm/year until the reduction of groundwater extraction after 2001.

480 Here, extensometer group four, which has long-term observation data of the
481 compaction of individual strata and variable drawdown, is taken as an example. There
482 are three aquitards, one unconfined aquifer, and four confined aquifers at
483 extensometer group four shown as in the stratigraphic distribution at the site of
484 extensometer group four (Figure 9). The unconfined aquifer (UA) was composed of
485 silty sand and buried from 0 m to 7 m below the ground surface, and could be
486 recharged directly by surface water. Therefore, the annual average water level in UA
487 has remained almost unchanged over years. The first confined aquifer (CA1) and the
488 second confined aquifer (CA2), which are mainly composed of sand, were primarily
489 pumped aquifers in this area and buried from 30 m to 48 m and 88 m to 153 m below
490 the ground surface, respectively. The hydraulic head of the CA1 and CA2 dropped by
491 5.0 m, and the yearly decline rates of the hydraulic head both are about 0.25 m/year
492 from 1981 to 2001. The total land subsidence during 1981–2001 was 226.48 mm, and
493 the cumulative compaction of aquitard 1 and aquitard 2 was 55.25 and 22.84 mm,
494 respectively, which is about 24.39% and 10.08% of the total subsidence during 1981–
495 2001 (Figure 10) (Shi et al., 2008).

496

497 **Figure 8. Location map and administrative divisions of Shanghai, and the locations of**
498 **extensometer groups modified from Li et al. (2021).**

499

500 **Figure 9. Physical and mechanical properties of soil layers (modified from Zhang et al.**
501 **(2007).**

502

503 **Figure 10. Groundwater level variations in confined aquifers, land subsidence, and**
504 **compaction of individual strata at extensometer group four modified from Zhang et al.**
505 **(2007).**

506 5.2 Determination of Aquitard Parameters

507 Due to the lack of specific compression distribution of each layer, the aquitard is
508 simplified as a homogeneous confining layer for analysis and treatment to determine
509 the overall average hydrogeological parameters over the whole thickness. The water
510 level of UA has remained almost unchanged over the period of 1981 – 2001, thus it is
511 inferred that the deformation of aquitard 1 was caused by the drawdown in CA1.
512 Meanwhile, the deformation of aquitard 2 was inferred to be caused by the drawdown
513 in CA1 and CA2. Therefore, aquitards 1 and 2 are regarded as the aquitard
514 undergoing drainage from one and both sides, respectively.

515 In order to determine the hydrogeological parameters of aquitards 1 and 2, we
516 only consider the drawdown history from 1981 to 2001 and divide 20 years of
517 drawdown history into 3 periods, each being Δt to be 6.67 years. Thus, we have
518 constant drawdowns during the 3 periods to be 1.6, 1.6, and 1.8 m, respectively,
519 leading to $\varphi_1^1 = 1.6$ m, $\varphi_2^1 = 1.6$ m, and $\varphi_3^1 = 1.8$ m, where the superscript 1 represents
520 aquitard 1. For aquitard 2, the stepped drawdown during the 3 periods in CA1 and
521 CA2 are: $\varphi_{0,1}^2 = \varphi_{1,1}^2 = 1.6$ m, $\varphi_{0,2}^2 = \varphi_{1,2}^2 = 1.6$ m, and $\varphi_{0,3}^2 = \varphi_{1,3}^2 = 1.8$ m,
522 respectively. In addition, parameters of the aquitard 1 and aquitard 2 are as follow:
523 $l^1 = 23$ m, $e_0^1 = 1.10$, $\sigma_0^{1'} = 150$ kPa, $l^2 = 40$ m, $e_0^2 = 0.93$, and $\sigma_0^{2'} = 610$ kPa.

524 Similar to section 3.1, the type-curve fitting method determines the
 525 hydrogeological parameters of the aquitard. The logarithmic forms of equation (15) in
 526 a dimensionless form ($\bar{Q}(\bar{t})$) and dimensionless time ($\Delta\bar{t} = \frac{c_v \Delta t}{l^2}$) are respectively
 527 expressed as:

$$\log_{10} \bar{Q}(\bar{t}) = \log_{10} Q(t) + \log_{10} \left[\frac{1 + e_0}{c_c l} \right] \#(22a)$$

$$\log_{10} \Delta\bar{t} = \log_{10} \Delta t + \log_{10} \frac{c_v}{l^2} \#(22b)$$

528 Because the value of c_v affects the dimensionless time ($\Delta\bar{t}$), we plotted the type
 529 curve under different $\Delta\bar{t}$ values and fitted the measured data with a type curve to
 530 determine the c_v value. The type curve of $\bar{Q}(\bar{t})$ under different $\Delta\bar{t}$ values is presented
 531 in Figure 11. In addition, we keep the final point of the measured data to coincide
 532 with the final point of the dimensionless curve, while superimposing $Q(t)$ curve over
 533 $\bar{Q}(\bar{t})$, and selecting the matching point as the intersection of the type curve and the
 534 $Q(t)$ data curve. Then, substitute the coordinates of the match points $Q(t)$ 、 $\bar{Q}(\bar{t})$ 、
 535 Δt and $\Delta\bar{t}$ into equations (26) and (27) to determine the hydrogeological parameters.

$$c_v = \frac{l^2 \Delta\bar{t}}{\Delta t} \#(23)$$

$$c_c = \frac{Q(t)(1 + e_0)}{\bar{Q}(\bar{t})l} \#(24)$$

536 The measured values of $Q(t)$ of aquitard 1 match the type-cure $\bar{Q}(\bar{t})$ of $\Delta\bar{t}$ is
 537 0.30, and its coordinates in the two systems are $Q = 2.6 \times 10^{-2} \text{ m}^3$, $\bar{Q} = 3.2 \times 10^{-2}$, $t = 12$
 538 years and $\bar{t} = 0.46$ (see Figure 9a). Substituting these values into equations (23) and
 539 (24) yields the estimated coefficient of consolidation, $c_{v1} = 7.62 \times 10^{-7} \text{ m}^2/\text{s}$, and the
 540 compression index, $c_{c1} = 0.074$, of aquitard 1. The S_s and k_v of the aquitard 1 at initial
 541 time respectively are $9.9 \times 10^{-4} \text{ m}^{-1}$ and $7.62 \times 10^{-10} \text{ m/s}$, which can be calculated by

542 $S_s = \frac{0.434\gamma_w C_c}{(1+e_0)\sigma'_0}$ and $k_v = \frac{0.434c_v C_c \gamma_w}{(1+e_0)\sigma'_0}$, respectively.

543 The measured values of $Q(t)$ of aquitard 2 match the type-curve $\bar{Q}(\bar{t})$ of $\Delta\bar{t}$ is
544 0.10, and its coordinates in the two systems are $Q = 1.26 \times 10^{-2} \text{ m}^3$, $\bar{Q} = 9.8 \times 10^{-2}$, $t =$
545 13 years and $\bar{t} = 0.18$ (see Figure 9b). The estimated coefficient of consolidation, c_{v2}
546 $= 7.57 \times 10^{-7} \text{ m}^2/\text{s}$, and the compression index, $C_{c2} = 0.063$, of aquitard 2. The S_s and k_v
547 of the aquitard 2 at an initial time are $2.3 \times 10^{-4} \text{ m}^{-1}$ and $1.75 \times 10^{-10} \text{ m/s}$, respectively.

548

549 **Figure 11. Determination of parameters by the type-curve fitting method: (a) aquitard 1; (b)**
550 **aquitard 2.**

551 5.3 Verification and Discussion

552 The above estimated hydrogeological parameters are substituted into the
553 equation (21) to obtain the estimated $Q(t)$ of aquitard 1 and aquitard 2 under the
554 condition of linear drawdown. Figure 12 shows the estimated and measured curves of
555 the $Q(t)$. In particular, the estimated and measured depletion of the aquitard 1 per unit
556 horizontal area respectively are 0.054 and 0.055 m^3 , while the corresponding error
557 value is 1.8%. The estimated and measured depletion of the aquitard 2 per unit
558 horizontal area respectively are 0.023 and 0.022 m^3 , while the corresponding error is
559 4.3%. It is seen that the depletion of the aquitard predicted by the analytical solution
560 in this study agrees well with the measured results, which means the accuracy of the
561 hydrogeological parameters determined by the proposed method.

562

563 **Figure 12. Comparison of predicted and measured settlement of the aquitard 1 and 2.**

564 The values of k_v and S_s , in fact, decrease with the increasing effective stress
565 with the development of consolidation of the aquitard. The estimated k_v and S_s at the
566 lower surface of aquitard 1 in 2001 were 5.71×10^{-10} m/s and 7.4×10^{-4} m⁻¹,
567 respectively. Similarly, the estimated k_v and S_s at the lower surface of aquitard 2 in
568 2001 were 1.69×10^{-10} m/s and 2.22×10^{-4} m⁻¹, respectively.

569 By comparing the estimated and measured k_v and S_s with the results of the
570 geologic method calibrated by Konikow & Neuzil (2007) (see Figure 13), the
571 estimated and measured k_v were close to the clay layer with medium content, which
572 is similar to the characteristics of clay in Shanghai (Zhang et al., 2007). It is found
573 that the k_v and S_s of aquitards 1 and 2 are less than laboratory experimental results
574 (Figure 9), due to the fact that both aquitards have experienced consolidation over a
575 very long time and under originally extremely high-stress conditions, while the
576 laboratory samples were inevitably subjected to stress perturbation due to many
577 factors such as sample collection, transportation and laboratory installation (Konikow
578 & Neuzil, 2007; Zhuang et al., 2015). The estimated S_s is closer to the soil parameters
579 of over-consolidated soil, which is because the aquitards have undergone
580 consolidation under greater effective stress caused by drawdown in the CA1 and CA2
581 before 1965.

582

583 **Figure 13. Comparison of predicted and measured hydraulic conductivity (a) and specific**
584 **storage (b) of the aquitard in the geologic method calibrated from Konikow & Neuzil (2007).**

585 **6. Conclusions**

586 In this study, the hydrogeological conceptual model of a multi-layer aquifer
 587 system is constructed. Based on the theories developed by Davis & Raymond (1965)
 588 and Gibson et al. (1967), the governing equation for nonlinear consolidation of an
 589 aquitard is developed without considering the creep effect. A general analytical
 590 solution under nonhomogeneous initial conditions and arbitrary boundary conditions
 591 is proposed to describe the variation of drawdown in the aquitard undergoing
 592 nonlinear consolidation. Based on the analytical solution, methods to calculate the
 593 hydrogeological parameters and long-term decreases in the volume of water stored in
 594 the low permeability aquitard undergoing nonlinear consolidation are put forward,
 595 under a condition that the drawdown history of the aquifers above and underlying the
 596 aquitard can be approximated as step-by-step piecewise function with respect to time.
 597 In addition, factors affecting the $Q(t)$ are also studied under the conditions of
 598 constant and linearly increasing drawdown in the adjacent confined aquifer. The new
 599 method proposed in this study is demonstrated by a laboratory experiment and a field
 600 application to the aquifer system beneath Shanghai city of China. The main
 601 conclusions are as follows:

602 (1) Under the condition of linear drawdown in adjacent aquifers, the depletion of
 603 the aquitard increases with increasing C_c, β, l, c_v and it decreases with increasing e_0 ,
 604 σ'_0 , while it becomes independent of c_v over long timescales. The $q(t)$ of the aquitard
 605 increases initially and then it gradually decreases. The effect of the parameter values
 606 on the $q(t)$ tends to disappear over long timescales. The maximum value of the water
 607 release rate increases with increasing C_c, φ, l, c_v and decreasing e_0, σ'_0 . The

608 occurrence time for the maximum value of $q(t)$ increases with increasing σ'_0 , l and
609 decreasing c_v , β and it does not depend on the value of C_c and e_0 .

610 (2) The proposed analytical method for calculating groundwater depletion of
611 aquitard, of which the error is generally less than 4%, is very good, and its accuracy is
612 better while the drawdown history of pumped aquifers is divided into more periods for
613 estimation. By comparing groundwater depletion of aquitard under the conditions of
614 linear drawdown and constant drawdown using “Representative time”, the results are
615 in good agreement, while the latter is slightly greater than the former.

616 (3) The estimated hydraulic parameters of the aquitards 1 and 2 at the selected
617 field site are closer to the data of the soil layer with moderate clay content and over-
618 consolidation, which is similar to the characteristics of clay found in Shanghai City,
619 and they are in general agreement with the results of the geologic method developed
620 by Konikow & Neuzil (2007). However, they are usually smaller than the
621 experimental results due to long-term consolidation and stress disturbance during the
622 test.

623 **Acknowledgments**

624 This study was financed by the Open Fund of State Key Laboratory of Geohazard
625 Prevention and Geoenvironment Protection (Chengdu University of Technology)
626 (SKLGP2021K023), the National Natural Science Foundation of China (41702253),
627 and the China Scholarship Council for working at the University of Waterloo as a
628 visiting scholar. Walter A. Illman appreciates the support of the Discovery Grant from
629 the National Science and Engineering Research Council of Canada (NSERC), which

630 made this collaboration possible.

631 **Data Availability Statement**

632 The test data in the section 3.1-3.2 is available through Luo et al. (2020). Data,
633 the parameter values in sections 4.1-4.3 is available through Li et al. (2019). Data, the
634 parameter values in sections 5.1-5.3, is available through Zhang et al. (2007) and
635 Konikow & Neuzil (2007).

636

637 **Appendix: Derivation of Equation (11)**

638 The mathematical statement of the problem consisting of equations (7) – (10)
639 are as follows:

$$640 \quad c_v \left[\frac{\partial^2 s}{\partial a^2} - \frac{\gamma_w}{\sigma'_0 + \gamma_w s} \left(\frac{\partial s}{\partial a} \right)^2 \right] = \frac{\partial s}{\partial t} \#(7)$$

$$641 \quad s(a, 0) = f(a) = 0 < a < l \#(8)$$

$$642 \quad s(0, t) = s_0(t) \quad t > 0 \#(9)$$

$$643 \quad s(l, t) = s_1(t) \quad t > 0 \#(10)$$

644 Using the substitution:

$$645 \quad w = \log_{10}(\sigma' / \sigma'_0) = \log_{10}((\sigma'_0 + \gamma_w s) / \sigma'_0) \quad (A1)$$

646 The boundary conditions are simplified by substituting equation (A1) into equations

647 (7) – (10) as follows:

$$c_v \frac{\partial^2 w}{\partial a^2} = \frac{\partial w}{\partial t} \#(A2)$$

$$w(a, 0) = \log_{10} \frac{\sigma'_0 + \gamma_w f(a)}{\sigma'_0} \quad 0 < a < l \#(A3)$$

$$w(0, t) = \log_{10} \frac{\sigma'_0 + \gamma_w s_1(t)}{\sigma'_0} \quad t > 0 \#(A4)$$

$$w(l, t) = \log_{10} \frac{\sigma'_0 + \gamma_w s_2(t)}{\sigma'_0} \quad t > 0 \#(A5)$$

648 Because boundary condition (A5) is non-homogeneous, it is necessary to simplify the
 649 boundary conditions as follows:

$$w(a, t) = p(a, t) + q(a, t) \#(A6)$$

$$q(a, t) = \log_{10} \frac{\sigma'_0 + \gamma_w s_1(t)}{\sigma'_0} + \frac{a}{l} \log_{10} \frac{\sigma'_0 + \gamma_w s_2(t)}{\sigma'_0 + \gamma_w s_1(t)} \#(A7)$$

650 Substituting $w(a, t)$ with $p(a, t)$ of equation (A2), the initial condition and boundary
 651 condition leads to:

$$c_v \frac{\partial^2 p}{\partial a^2} - \frac{1}{\ln 10} \left(\frac{\gamma_w}{\sigma'_0 + \gamma_w s_1(t)} \frac{\partial s_1(t)}{\partial t} \left(1 - \frac{a}{l} \right) + \frac{\gamma_w}{\sigma'_0 + \gamma_w s_2(t)} \frac{\partial s_2(t)}{\partial t} \frac{a}{l} \right) = \frac{\partial p}{\partial t} \#(A8)$$

$$653 \quad p(a, 0) = \log_{10} \frac{\sigma'_0 + \gamma_w f(a)}{\sigma'_0} - \log_{10} \frac{\sigma'_0 + \gamma_w s_1}{\sigma'_0} - \frac{a}{l} \log_{10} \frac{\sigma'_0 + \gamma_w s_2}{\sigma'_0 + \gamma_w s_1} \quad 0 < a < l \#(A9)$$

$$654 \quad p(0, t) = 0 \quad 0 < a < l \#(A10)$$

$$655 \quad p(l, t) = 0 \quad 0 < a < l \#(A11)$$

656 where s_1, s_2 are the drawdown in the aquifers lying respectively above and below the
 657 aquitard at the initial time ($t=0$), respectively.

658 The solution of equations (A8) – (A11) was derived using the separation of
 659 variables method as:

$$p(a, t) = \sum_{n=1}^{\infty} [T_n(0) e^{-\frac{n^2 \pi^2 c_v t}{l^2}} + e^{-\frac{n^2 \pi^2 c_v t}{l^2}} \int_0^t f_n(t) e^{\frac{n^2 \pi^2 c_v t}{l^2}} dt] \sin \frac{n \pi a}{l} \#(A12)$$

660 where

$$f_n(t) = \frac{2}{n \pi \ln 10} \left[\frac{(-1)^n \gamma_w}{\sigma'_0 + \gamma_w s_2(t)} \frac{\partial s_2(t)}{\partial t} - \frac{\gamma_w}{\sigma'_0 + \gamma_w s_1(t)} \frac{\partial s_1(t)}{\partial t} \right] \#(A13)$$

$$T_n(0) = \frac{2}{l} \int_0^l \log_{10} \frac{\sigma'_0 + \gamma_w f(a)}{\sigma'_0} \sin \frac{n \pi a}{l} da + \frac{2}{n \pi} \left(\log_{10} \frac{\sigma'_0 + \gamma_w s_2}{\sigma'_0} (-1)^n - \log_{10} \frac{\sigma'_0 + \gamma_w s_1}{\sigma'_0} \right) \#(A14)$$

661 Combining (A7) with (A12) to obtain the solution of equations (A2) – (A5) leads to,

$$w(a, t) = \sum_{n=1}^{\infty} \left[T_n(0) e^{-\frac{n^2 \pi^2 c_v t}{l^2}} + e^{-\frac{n^2 \pi^2 c_v t}{l^2}} \int_0^t f_n(t) e^{\frac{n^2 \pi^2 c_v t}{l^2}} dt \right] \sin \frac{n \pi a}{l} + \log_{10} \frac{\sigma'_0 + \gamma_w s_1(t)}{\sigma'_0} + \frac{a}{l} \log_{10} \frac{\sigma'_0 + \gamma_w s_2(t)}{\sigma'_0 + \gamma_w s_1(t)} \#(A15)$$

662 The solution of equation (11) was derived by substituting equation (A15) into
663 equation (A1).

664 **References**

- 665 Arabameri, A., Saha, S., Roy, J., Tiefenbacher, J. P., Cerda, A., Biggs, T., Pradhan, B., Thi Ngo, P. T. &
666 Collins, A. L. (2020). A novel ensemble computational intelligence approach for the spatial
667 prediction of land subsidence susceptibility. *Science of the Total Environment* 726(C), 637-
668 653. <https://doi.org/10.1016/j.scitotenv.2020.138595>
- 669 Bakr, M. (2015). Influence of Groundwater Management on Land Subsidence in Deltas:A Case Study
670 of Jakarta (Indonesia). *Water Resources Management* 29(5), 1541-1555.
671 <https://doi.org/10.1007/s11269-014-0893-7>
- 672 Burbey, T. J. (2003). Use of time–subsidence data during pumping to characterize specific storage and
673 hydraulic conductivity of semi-confining units. *Journal of Hydrology* 281(1), 3-22.
674 [https://doi.org/10.1016/S0022-1694\(03\)00197-5](https://doi.org/10.1016/S0022-1694(03)00197-5)
- 675 Burbey, T. J. (2020). Parameter estimation of a multiple aquifer-aquitard system from a single
676 extensometer record: Las Vegas, Nevada, USA. *Proceedings of the International Association*
677 *of Hydrological Sciences* 382, 51-56. <https://doi.org/10.5194/piahs-382-51-2020>
- 678 Chai, J., Shen, S., Zhu, H. & Zhang, X. (2004). Land subsidence due to groundwater drawdown in
679 Shanghai. *Géotechnique* 54(2), 143-147. <https://doi.org/10.1680/geot.2004.54.2.143>
- 680 Custodio, E. (2002). Aquifer overexploitation: what does it mean? *Hydrogeology journal* 10(2), 254-
681 277. <https://doi.org/10.1007/s10040-002-0188-6>
- 682 Davis, E. H. & Raymond, G. P. (1965). A Non-Linear Theory of Consolidation. *Géotechnique* 15(2),
683 161-173. <https://doi.org/10.1680/geot.1965.15.2.161>

684 Gibson, R. E., England, G. L. & Hussey, M. J. L. (1967). The Theory of One-Dimensional
685 Consolidation of Saturated Clays. *Géotechnique* 17(3), 261-273.
686 <https://doi.org/10.1680/geot.1967.17.3.261>

687 Gibson, R. E., Schiffman, R. L. & Cargill, K. W. (1981). The theory of one-dimensional consolidation
688 of saturated clays. II. Finite nonlinear consolidation of thick homogeneous layers. *Canadian*
689 *Geotechnical Journal* 18(2), 143-144. <https://doi.org/10.1139/t81-030>

690 Guo, Q. & Li, H. (2015). Terrestrial-originated submarine groundwater discharge through deep
691 multilayered aquifer systems beneath the seafloor. *Hydrological Processes* 29(2), 295-309.
692 <https://doi.org/10.1002/hyp.10163>

693 Konikow, L. F. & Kendy, E. (2005). Groundwater depletion: A global problem. *Hydrogeology Journal*
694 13(1), 317-320. <https://doi.org/10.1007/s10040-004-0411-8>

695 Konikow, L. F. & Neuzil, C. E. (2007). A method to estimate groundwater depletion from confining
696 layers. *Water Resources Research* 43(7). <https://doi.org/10.1029/2006WR005597>

697 Li, M., Chen, J., Xu, Y., Tong, D., Cao, W. & Shi, Y. (2021). Effects of groundwater exploitation and
698 recharge on land subsidence and infrastructure settlement patterns in Shanghai. *Engineering*
699 *Geology* 282. <https://doi.org/10.1016/j.enggeo.2021.105995>

700 Li, Z. & Zhou, Z. (2015). An analytical solution for leakage rate and depletion of aquitard influenced
701 by the delayed yield phenomenon. *Environmental Earth Sciences* 74(2), 1227-1234.
702 <https://doi.org/10.1007/s12665-015-4114-3>

703 Li, Z., Zhou, Z., Chen, Z., Liu, G. & Zhou, C. (2017). An analytical method to estimate groundwater
704 depletion from a confining layer. *Natural Hazards* 85(2), 887-906.
705 <https://doi.org/10.1007/s11069-016-2609-1>

706 Li, Z., Zhou, Z., Dai, Y. & Dai, B. (2019). Contaminant transport in a largely-deformed aquitard
 707 affected by delayed drainage. *Journal of Contaminant Hydrology* 221, 118-126.
 708 <https://doi.org/10.1016/j.jconhyd.2019.02.002>

709 Li, Z., Zhou, Z., Li, M., Zhang, B., Dai, B. & Bai, Q. (2018). Delayed Drainage of a Largely Deformed
 710 Aquitard due to Abrupt Water Head Decline in Adjacent Aquifer. *Geofluids* 2018.
 711 <https://doi.org/10.1155/2018/2326491>

712 Liu, C., Shi, B., Gu, K., Zhang, T., Tang, C., Wang, Y. & Liu, S. (2022). Negative Pore Water Pressure
 713 in Aquitard Enhances Land Subsidence: Field, Laboratory, and Numerical Evidence. *Water*
 714 *Resources Research* 58(1), e2021WR030085. <https://doi.org/10.1029/2021WR030085>

715 Luo, H., Li, Z., Luo, M., Zhang, Q. & Illman, W. A. (2020). An analytical method to calculate
 716 groundwater released from an aquitard undergoing nonlinear consolidation. *Water Resources*
 717 *Research* 56(9). <https://doi.org/10.1029/2020wr027320>

718 Neuman, S. P. & Gardner, D. A. (1989). Determination of Aquitard/Aquiclude Hydraulic Properties
 719 from Arbitrary Water-Level Fluctuations by Deconvolution. *Groundwater* 27(1), 66-76.
 720 <https://doi.org/10.1111/j.1745-6584.1989.tb00009.x>

721 Neuman, S. P. & Witherspoon, P. A. (1969). Applicability of Current Theories of Flow in Leaky
 722 Aquifers. *Water Resources Research* 5(4), 817-829.
 723 <https://doi.org/10.1029/WR005i004p00817>

724 Shi, X., Wu, J., Xue, Y., Zhang, Y., Wei, Z. & Yu, J. (2007). The development and control of the land
 725 subsidence in the Yangtze Delta, China. *Environmental Geology* 55(8), 1725-1735.
 726 <https://doi.org/10.1007/s00254-007-1123-x>

727 Shi, X., Xue, Y., Wu, J., Ye, S., Zhang, Y., Wei, Z. & Yu, J. (2008). Characterization of regional land

728 subsidence in Yangtze Delta, China: the example of Su-Xi-Chang area and the city of
 729 Shanghai. *Hydrogeology Journal* 16(3), 593-607. <https://doi.org/10.1007/s10040-007-0237-2>

730 Terzaghi, K. (1943) *Theoretical Soil Mechanics*, New York: Wiley.

731 Xie, K. & Leo, C. J. (2004). Analytical solutions of one-dimensional large strain consolidation of
 732 saturated and homogeneous clays. *Computers and Geotechnics* 31(4), 301-314.
 733 <https://doi.org/10.1016/j.compgeo.2004.02.006>

734 Ye, S., Xue, Y., Wu, J., Yan, X. & Yu, J. (2016). Progression and mitigation of land subsidence in
 735 China. *Hydrogeology Journal* 24(3), 685-693. <https://doi.org/10.1007/s10040-015-1356-9>

736 Zhang, X., Wang, J., Wong, H., Leo, C., Liu, Q., Tang, Y., Yan, X., Sun, W., Huang, Z. & Hao, X.
 737 (2013). Land subsidence caused by internal soil erosion owing to pumping confined aquifer
 738 groundwater during the deep foundation construction in Shanghai. *Natural Hazards* 69(1),
 739 473-489. <https://doi.org/10.1007/s11069-013-0718-7>

740 Zhang, Y., He, G., Wu, J., Zhu, Z., Yan, X. & Yang, T. (2020a). Experimental study on mechanism for
 741 pumping-induced land subsidence. *Proceedings of the International Association of*
 742 *Hydrological Sciences* 382, 387-390. <https://doi.org/10.5194/piahs-382-387-202>

743 Zhang, Y., Wu, J., Xue, Y., Wang, Z., Yao, Y., Yan, X. & Wang, H. (2015). Land subsidence and uplift
 744 due to long-term groundwater extraction and artificial recharge in Shanghai, China.
 745 *Hydrogeology Journal* 23(8), 1851-1866. <https://doi.org/10.1007/s10040-015-1302-x>

746 Zhang, Y., Xue, Y. & Wu, J. (2007). Stress-Strain Measurements of Deforming Aquifer Systems that
 747 Underlie Shanghai, China. *Environmental & Engineering Geoscience* 13(3), 218-228.
 748 <https://doi.org/10.2113/gsegeosci.13.3.217>

749 Zhang, Y., Yan, X., Yang, T., Wu, J. & Wu, J. (2020b). Three-Dimensional Numerical Investigation of

750 Pore Water Pressure and Deformation of Pumped Aquifer Systems. *Ground water* 58(2), 278-
751 290. <https://doi.org/10.5194/piahs-382-387-2020>

752 Zhao, Z., Illman, W. A., Zha, Y., Yeh, T. C. J., Mok, C. M. B., Berg, S. J. & Han, D. (2019). Transient
753 Hydraulic Tomography Analysis of Fourteen Pumping Tests at a Highly Heterogeneous
754 Multiple Aquifer–Aquitard System. *Water* 11(9). <https://doi.org/10.3390/w11091864>

755 Zhou, Z., Guo, Q. & Dou, Z. (2013). Delayed drainage of aquitard in response to sudden change in
756 groundwater level in adjacent confined aquifer: Analytical and experimental studies. *Chinese*
757 *Science Bulletin* 58(25), 3060-3069. <https://doi.org/10.1007/s11434-013-5730-5>

758 Zhuang, C., Zhou, Z., Zhan, H. & Wang, G. (2015). A new type curve method for estimating aquitard
759 hydraulic parameters in a multi-layered aquifer system. *Journal of Hydrology* 527, 212-220.
760 <https://doi.org/10.1016/j.jhydrol.2015.04.062>

761

Figure 1.

Unconfined or confined aquifer

$$s(0, t) = s_0(t)$$

0

Aquitard (C_c, e_0, C_v, σ'_0)

l

$$s(a, 0) = f(a)$$

Confined aquifer

$$s(l, t) = s_1(t)$$

a



Figure 2.

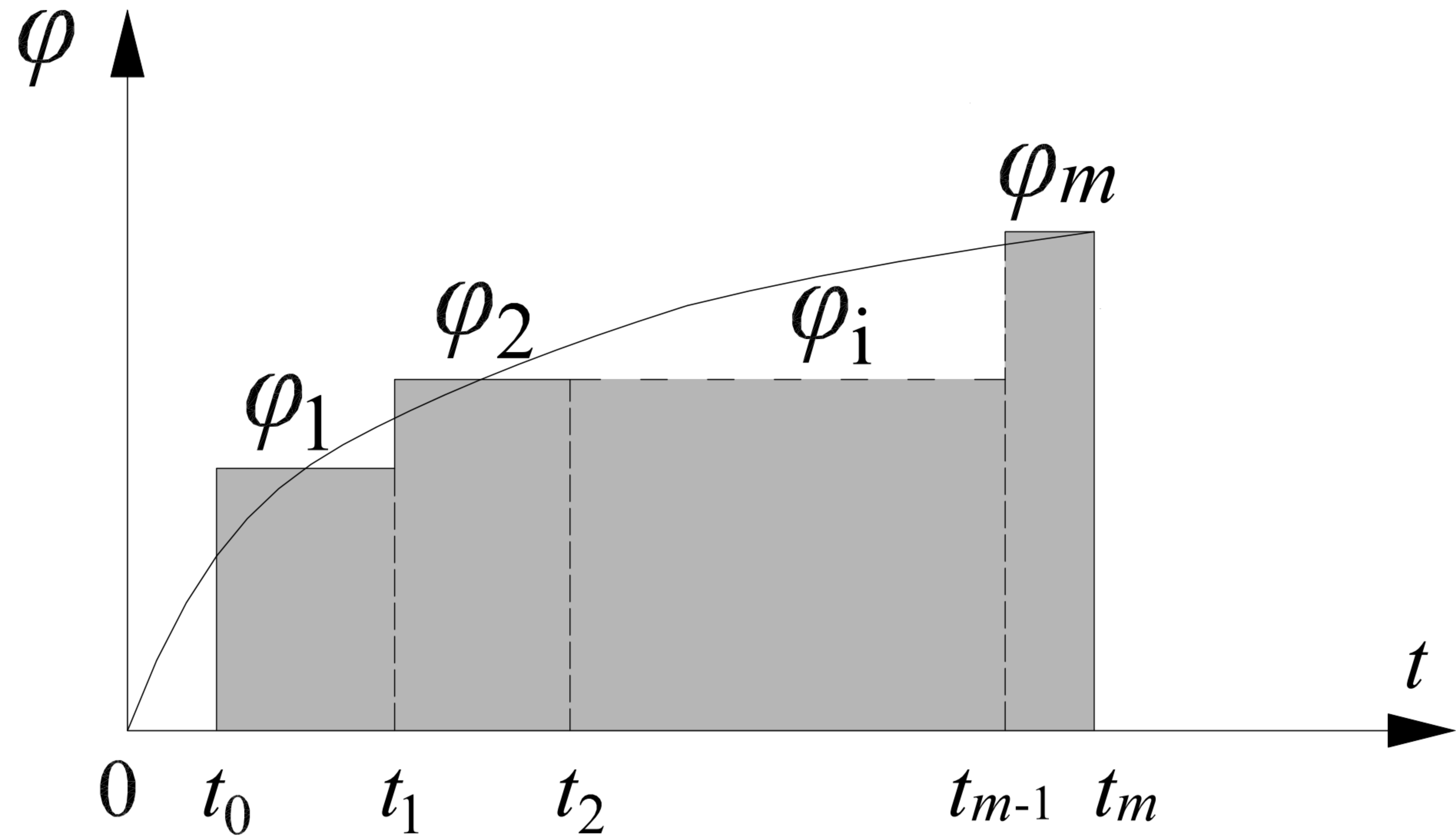


Figure 3.

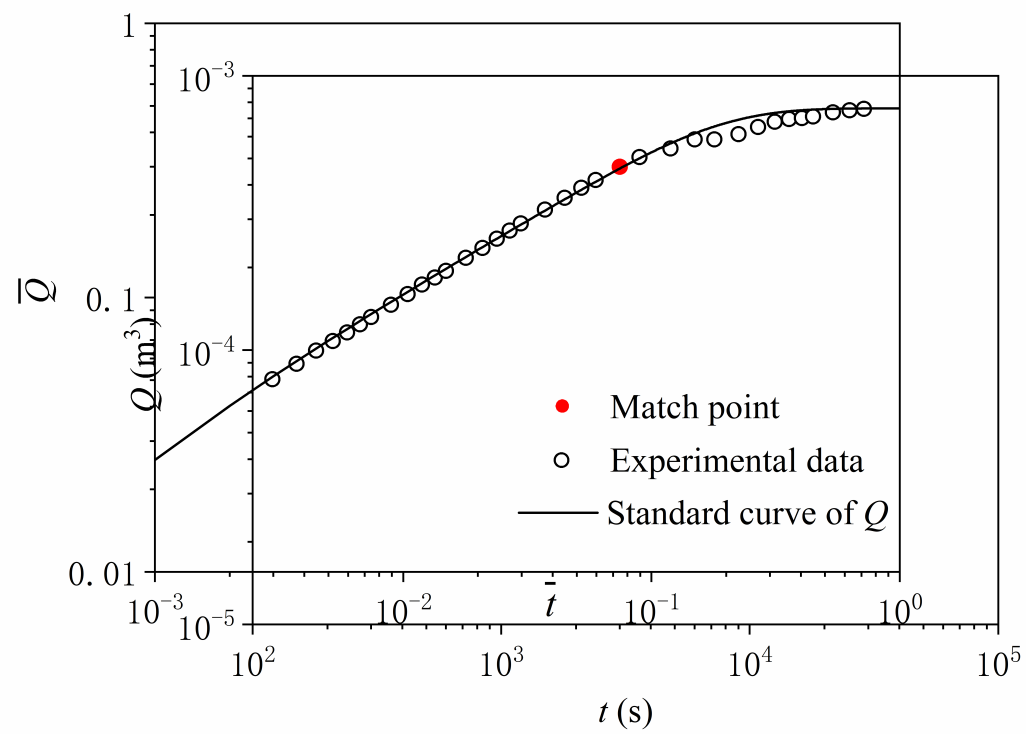


Figure 4.

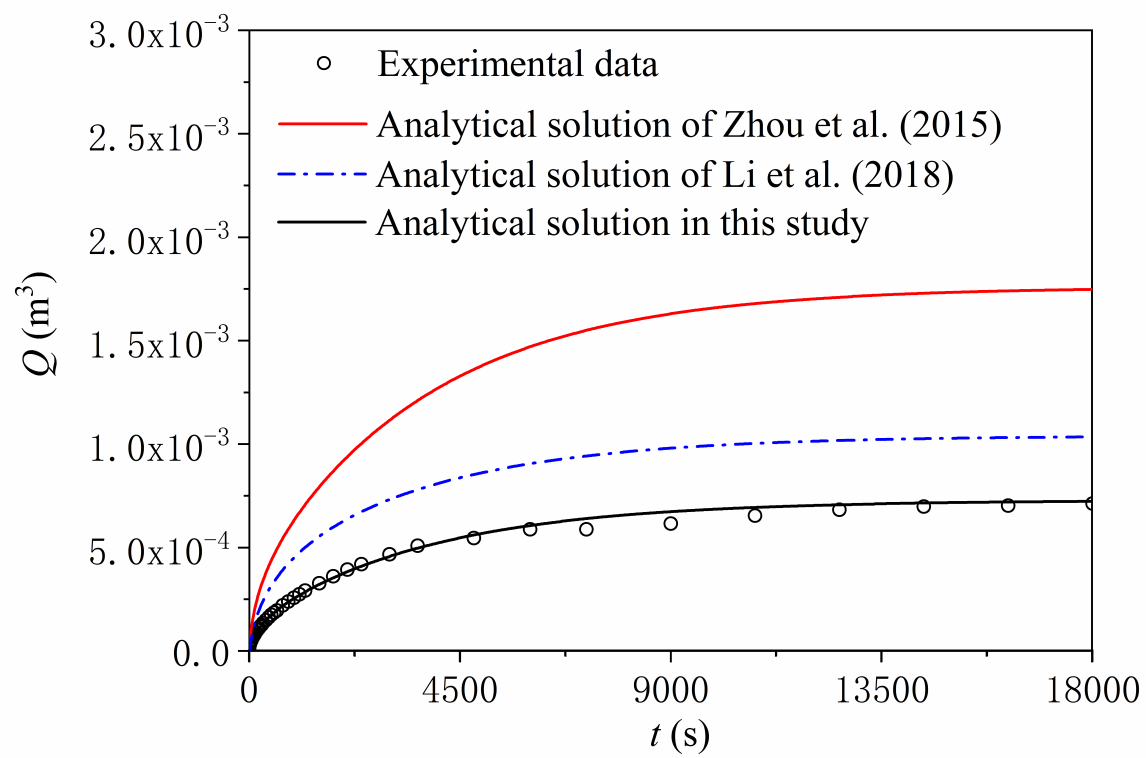


Figure 5.

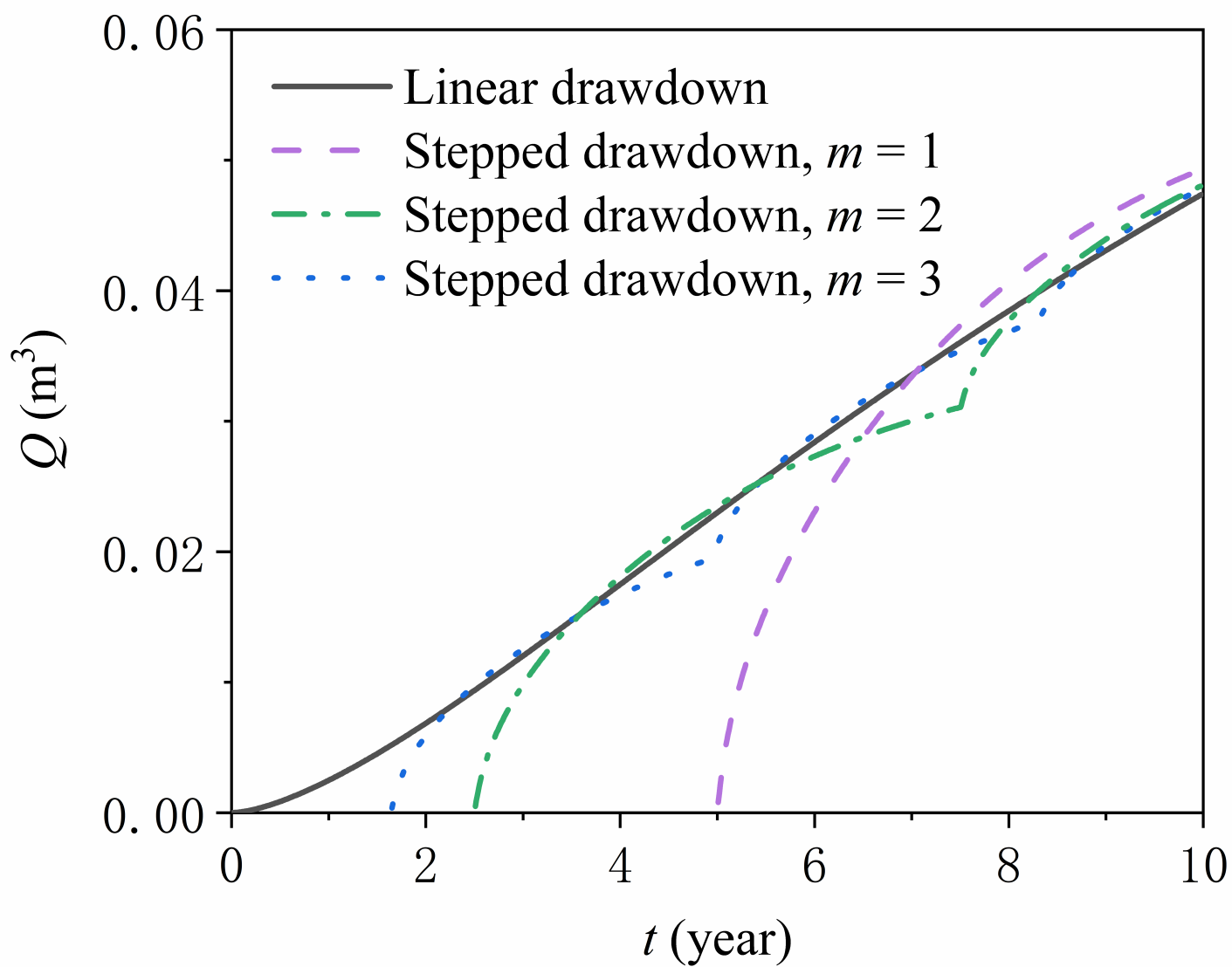


Figure 6.

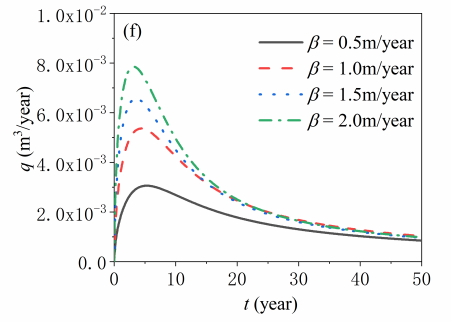
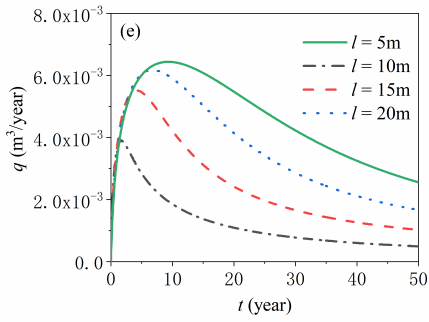
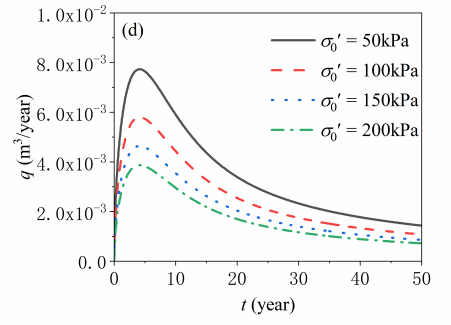
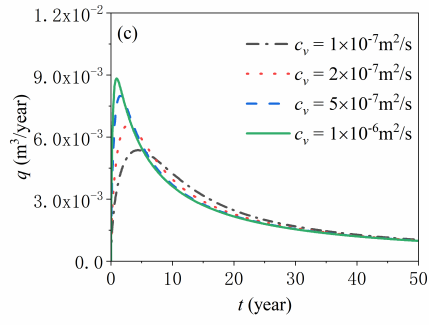
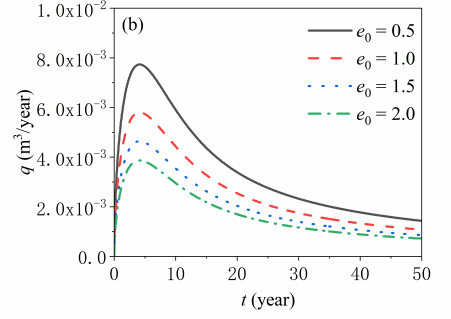
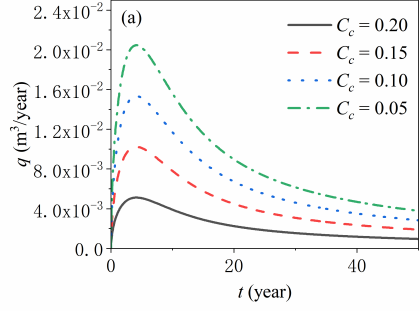
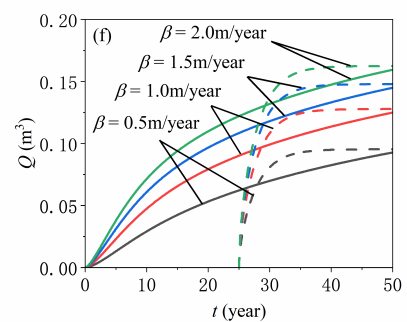
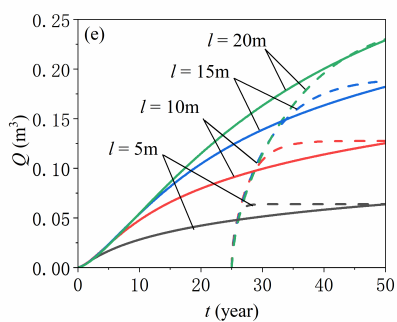
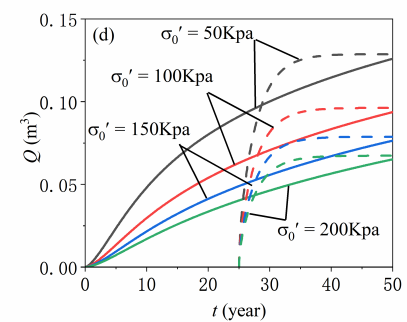
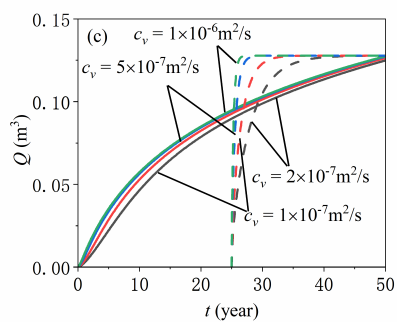
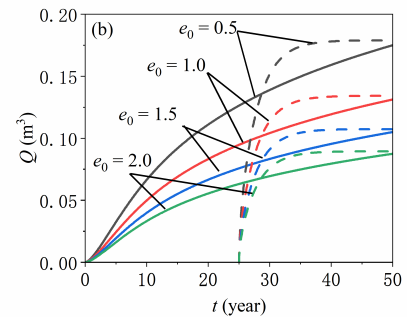
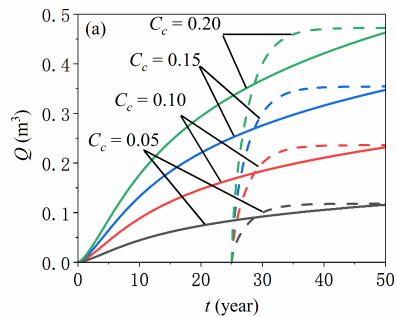


Figure 7.



— linear drawdown - - - fixed drawdown

Figure 8.

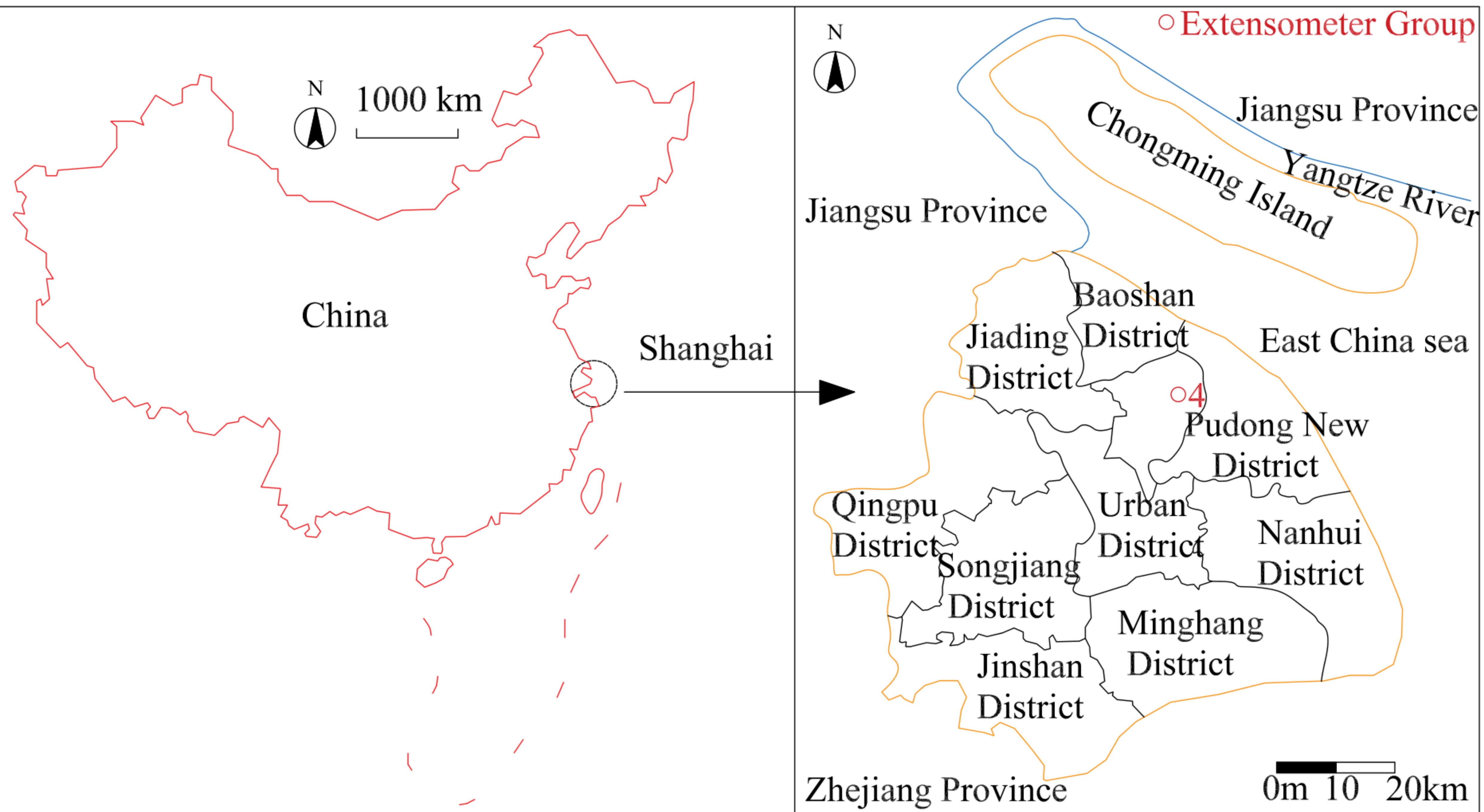


Figure 9.

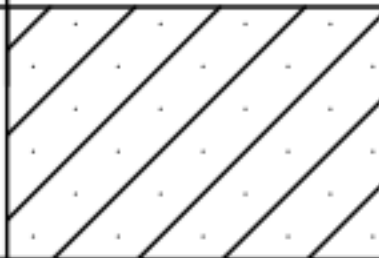
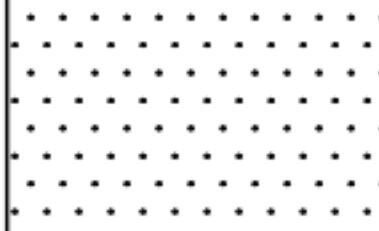
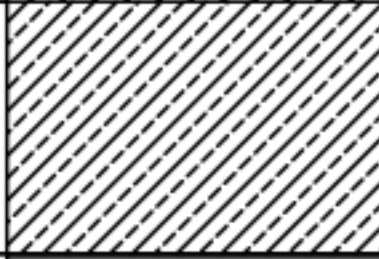

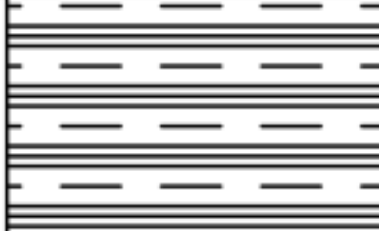
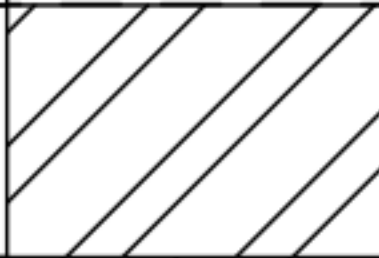
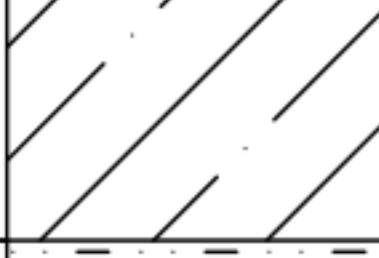
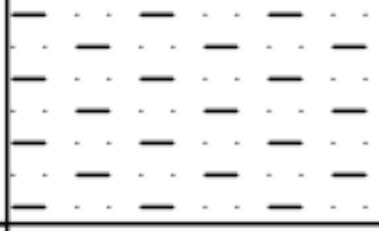
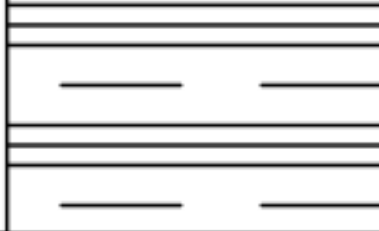
Depth interval (m)	Cross section	Soil types	Unit Weight (kN/m ³)	Void Ratio	Coefficient of Compression(MPa ⁻¹)	Hydraulic Conductivity(10 ⁻⁹ m/s)	Hydrogeological Stratigraphy
0~7		Sand layer one	17.5~19.2	0.83~1.23	0.29~0.65	21500	UA
7~24		Soft clay layer one and two	16.4~19.3	0.70~1.44	0.40~1.50	2.0	Aquitard 1
24~30		Hard clay layer two	20.2	0.66~0.70	0.21~0.35	1.34	Aquitard 1
30~48		Sand layer two	19.1~20.1	0.63~0.81	0.12~0.32	35000	CA1
48~88		Soft clay layer three	18.2~19.3	0.78~1.08	0.34~0.62	2.99	Aquitard 2
88~153		Sand layer three	19.1~21.2	0.43~0.82	0.26~0.45	41000	CA2
153~173		Hard clay layer three	19.7~20.5	0.66~0.86	0.07~0.25	0.13	Aquitard 3
174~239		Sand layer four	18.7~19.3	0.85~0.87	0.25~0.63	18100	CA3
239~333		Hard clay layer four	19.3~20.3	0.59~0.68	0.06~0.41	0.38	Aquitard 4

Figure 10.

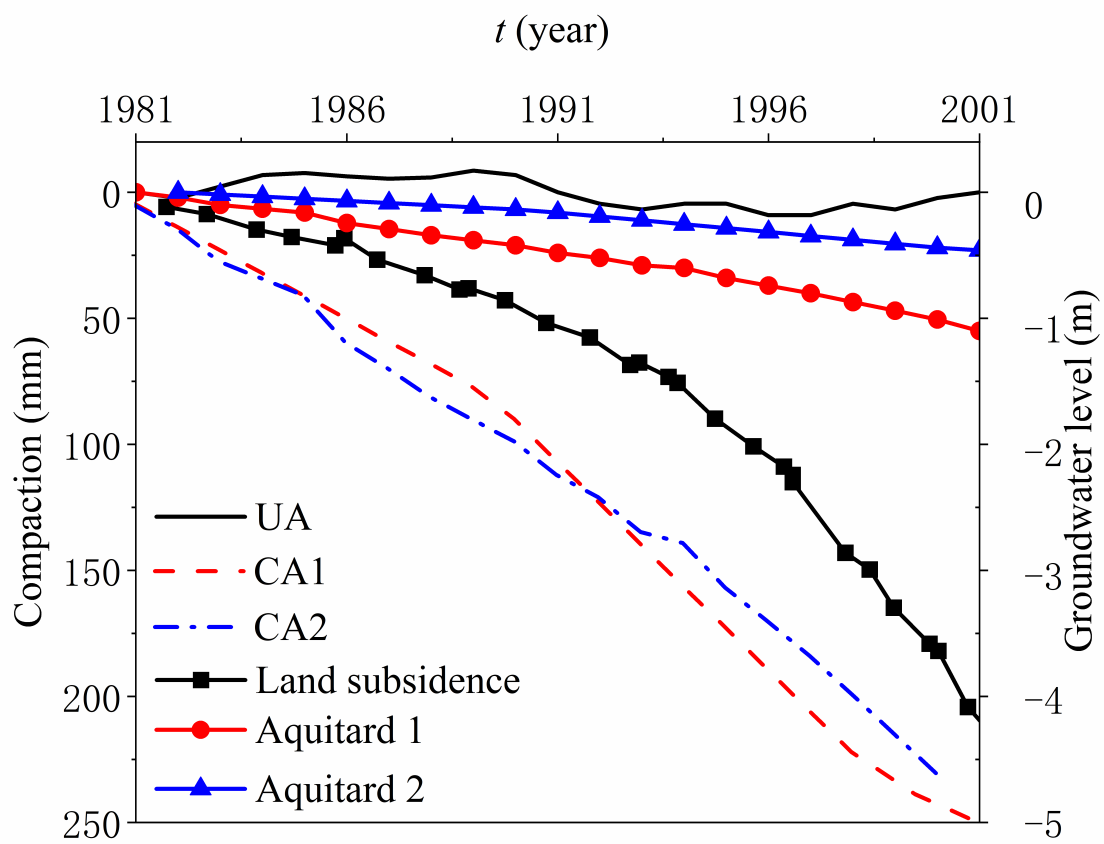


Figure 11.

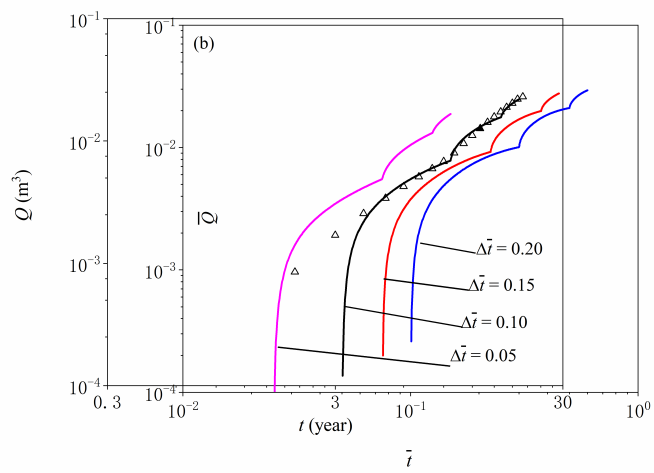
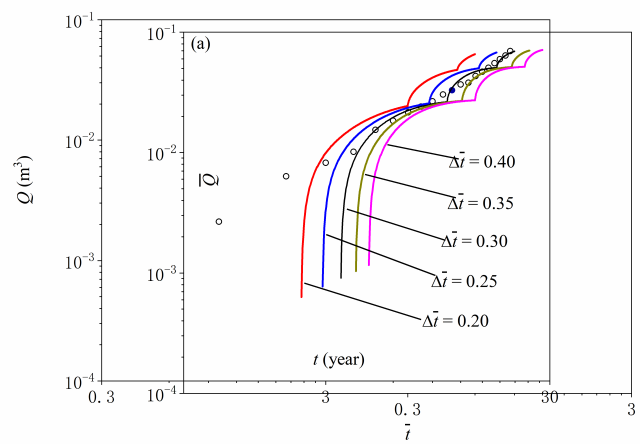


Figure 12.

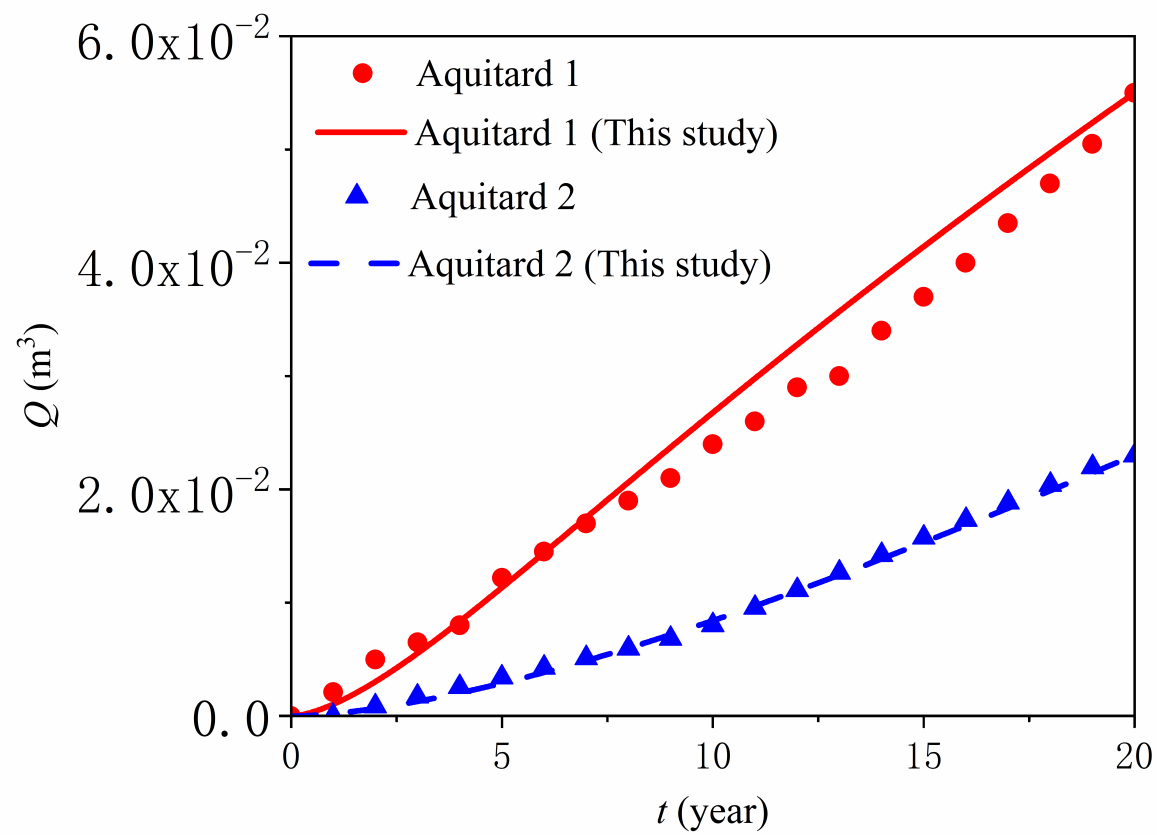


Figure 13.

